International Journal of Physical Sciences

Academic Journals

ABOUT IJPS

The **International Journal of Physical Sciences (IJPS)** is published weekly (one volume per year) by Academic Journals.

International Journal of Physical Sciences (IJPS) is an open access journal that publishes high-quality solicited and unsolicited articles, in English, in all Physics and chemistry including artificial intelligence, neural processing, nuclear and particle physics, geophysics, physics in medicine and biology, plasma physics, semiconductor science and technology, wireless and optical communications, materials science, energy and fuels, environmental science and technology, combinatorial chemistry, natural products, molecular therapeutics, geochemistry, cement and concrete research, metallurgy, crystallography and computer-aided materials design. All articles published in IJPS are peer-reviewed.

Contact Us

Editorial Office: ijps@academicjournals.org

Help Desk: helpdesk@academicjournals.org

Website: http://www.academicjournals.org/journal/IJPS

Submit manuscript online   http://ms.academicjournals.me/.

International Journal of Physical Sciences

ARTICLES

Full Length Research Paper

The first integral method and its application for finding the exact solutions of nonlinear fractional partial differential equations (PDES) in the mathematical physics

Elsayed M. E. Zayed* and Yasser A. Amer

Department of Mathematics, Faculty of Sciences, Zagazig University, Zagazig, Egypt.

In this article we apply the first integral method to construct the exact solutions of some nonlinear fractional partial differential equations (PDES) in the sense of modified Riemann–Liouville derivatives, namely the nonlinear fractional Zoomeron equation and the nonlinear fractional Klein- Gordon-Zakharov system of equations. Based on a nonlinear fractional complex transformation, these two nonlinear fractional equations can be turned into nonlinear ordinary differential equations (ODE) of integer order. This method has more advantages: it is direct and concise.

Key words: First integral method, exact solutions, nonlinear fractional Zoomeron equation, nonlinear fractional Klein-Gordon-Zakharov system of equations.

INTRODUCTION

Fractional differential equations have been the focus of many studies due to there frequent appearance in various applications in physics, biology, engineering, signal processing, systems identification, control theory, finance and fractional dynamics (Miller and Ross, 1993; Kilbas et al., 2006; Podlubny, 1999). Recently, a large amount of literature has been provided to construct the solutions of fractional ordinary differential equations, integral equations and fractional partial differential equations of physical interest. Several powerful methods have been proposed to obtain approximate and exact solutions of fractional differential equations, such as the Adomian decomposition method (El-Sayed et al., 2009; Safari et al., 2009), the variational iteration method (Inc, 2008; Wu and Lee, 2010; Fouladi et al., 2010), the homotopy analysis method (Song and Zhang, 2009;

Abbasbanby and Shirzadi, 2010; Barania et al., 2010; Rashidi et al., 2009), the homotopy perturbation method (Ganji et al., 2010; Gepreel, 2011; Gupta and Singh, 2011), the Lagrange characteristic method (Jumarie, 2006a), the fractional sub-equation method (Zhang and Zhang, 2001), the local fractional variation iteration method (Yang and Baleanu, 2013; Liu et al., 2013; Wang et al., 2014; Zhao et al., 2014; Baleanu et al., 2014; He, 2012; Yang et al., 2013; Yang et al., 2013) and so on.

Jumarie (2006b) proposed a modified Riemann-Liouville derivative. With this kind of fractional derivative and some useful formulas, we can convert fractional differential equations into integer-order differential equations by using variable transformations. The first integral method (Feng and Roger, 2007; Feng, 2008; Raslan, 2008; Lu et al., 2010; Taghizadeh et al., 2011) can be used to construct the exact solutions for some time fractional differential equations.

The objective of this paper is to investigate the applicability and effectiveness of the first integral method on fractional nonlinear partial differential equations, namely the nonlinear fractional Zoomeron equation and the nonlinear fractional Klein- Gordon- Zakharov system of equations.

The modified Riemann-Liouville derivative and first integral method

Here, we first give some definitions and properties of the modified Riemann-Liouville derivative which are used further in this paper. Assume that $f : R \to R$, $x \to f(y)$ denote a continuous (but not necessarily differentiable) function. The Jumarie's modified Riemann-Liouville derivative of order α is defined by the following expression:

$$
D_x^{\alpha} f(x) = \begin{cases} \dfrac{1}{\Gamma(-\alpha)} \displaystyle\int_0^x (x-\xi)^{-\alpha-1}[f(\xi)-f(0)]d\xi, & \alpha < 0, \\[2ex] \dfrac{1}{\Gamma(1-\alpha)} \dfrac{d}{dx} \displaystyle\int_0^x (x-\xi)^{-\alpha-1}[f(\xi)-f(0)]d\xi, & 0 \le \alpha < 1, \\[2ex] \left[f^{(n)}(x)\right]^{(\alpha-n)}, & n \le \alpha < n+1, n \ge 1 \end{cases}
$$

(1)

Some properties of the fractional modified Riemann-Liouville derivative were summarized and three useful formulas of them are:

$$
D_x^{\alpha} x^{\gamma} = \frac{\Gamma(1+\gamma)}{\Gamma(1+\gamma-\alpha)} x^{\gamma-\alpha}, \ \gamma > 0,
$$

(2)

$$
D_x^{\alpha}[f(x)g(x)] = f(x)D_x^{\alpha}g(x) + g(x)D_x^{\alpha}f(x),
$$

(3)

$$
D_x^{\alpha}[f(g(x))] = f_g'(g(x))D_x^{\alpha}g(x) = D_g^{\alpha}f(g(x))[g_x'(x)]^{\alpha}
$$

(4)

which are consequences of the equation $d^{\alpha}x(t) = \Gamma(1+\alpha)dx(t)$.

Next, let us consider the following time fractional differential equation with independent variables $x = (x_1, x_2, ..., x_m, t)$ and a dependent variable u:

$$
F(u, D_t^{\alpha}u, u_{x_1}, u_{x_2}, u_{x_3}, D_t^{2\alpha}u, u_{x_1 x_1}, u_{x_2 x_2}, ...) = o.
$$

(5)

Using the fractional complex transformation

$$
u(x_1, x_2, x_3, ..., x_m, t) = u(\xi), \quad \xi = x_1 + k_1 x_2 + ... + k_{m-1} x_m + \frac{ct^{\alpha}}{\Gamma(1+\alpha)}
$$

(6)

where k_i, c are constants to be determined later; the fractional Equation (5) is reduced to the nonlinear ODE of integer orders:

$$
H(u, u', u'', ...) = 0,
$$

(7)

where $u' = \dfrac{du}{d\xi}, u'' = \dfrac{d^2 u}{d\xi^2}, ...$.

We assume that Equation (7) has a solution in the form

$$
u(\xi) = X(\xi),
$$

(8)

and introduce a new independent variable $Y(\xi) = X'(\xi)$ which leads to a new system of equations

$$
\begin{aligned} X'(\xi) &= Y(\xi), \\ Y'(\xi) &= G(X(\xi), Y(\xi)). \end{aligned}
$$

(9)

Now, let us recall the first integral method. By using the division theorem for two variables in the complex domain C[X,Y] which is based on the Hilbert-Nullstellensatz Theorem (Bourbak, 1972), we can obtain one first integral to Equation (9) which can reduce Equation (7) to a first- order integrable ordinary differential equation. An exact solution to Equation (5) is obtained by solving this equation directly.

Division theorem

Suppose that $P(x,y)$ and $Q(x,y)$ are polynomials in C[X,Y] and $P(x,y)$ is irreducible in C[X,Y]. IF $Q(x,y)$ vanishes at all zero points of $P(x,y)$, then there exists a polynomial $H(x,y)$ in C[X,Y] such that

$$Q(x,y) = P(x,y)H(x,y).$$ (10)

Applications

Here, we present two examples to illustrate the applicability of the first integral method to solve nonlinear fractional partial differential equations.

Example 1. The nonlinear fractional Zoomeron equation

This equation is well-known (Alquran and Al-Khaled, 2012; Abazar, 2011) and can be written in the form:

$$D_{tt}^{2\alpha}[\frac{u_{xy}}{u}] - [\frac{u_{xy}}{u}]_{xx} + 2D_t^{\alpha}[u^2]_x = 0, \ 0 < \alpha \le 1.$$ (11)

For our purpose, we introduce the following transformations

$$u(x,y,t) = u(\xi), \ \xi = \ell x + cy - \frac{\omega t^{\alpha}}{\Gamma(1+\alpha)},$$ (12)

where ℓ, c, ω are constants. Substituting Equation (12) into (11), we have the ODE:

$$\ell c \omega^2 \left(\frac{u''}{u}\right)'' - c\ell^3 \left(\frac{u''}{u}\right)'' - 2\ell\omega(u^2)'' = 0$$ (13)

Integrating Equation (13) twice with respect to ξ, we get

$$\ell c(\omega^2 - \ell^2)u'' - 2\ell\omega u^3 - ru = 0$$ (14)

where *r* is a non zero constant of integration, while the second constant of integration is vanishing.
On using Equations (8) and (9), then Equation (14) is equivalent to the two dimensional autonomous system:

$$X'(\xi) = Y(\xi)$$ (15)

$$Y'(\xi) = \frac{rX(\xi) + 2\ell\omega X^3(\xi)}{\ell c(\omega^2 - \ell^2)},$$ (16)

where $X(\xi) = u(\xi)$.
According to the first integral method, we suppose that $X(\xi)$ and $Y(\xi)$ are nontrivial solutions of Equations (15) and (16) and $Q(X,Y)$ is an irreducible polynomial in the complex domain C[X.Y] such that

$$Q(X,Y) = \sum_{i=0}^{m} a_i(X)Y^i(\xi) = 0$$ (17)

where $a_i(X), \ (i = 1,2,...m)$ are polynomials in X and $a_m(X) \ne 0$. Due to the Division theorem, there exists a polynomial $[g(X) + h(X)Y(\xi)]$ in the complex domain C[X,Y] such that

$$\frac{dQ}{d\xi} = \frac{\partial Q}{\partial X}\frac{dX}{d\xi} + \frac{\partial Q}{\partial Y}\frac{dY}{d\xi} = [g(X) + h(X)Y(\xi)]\sum_{i=0}^{m} a_i(X)Y^i(\xi)$$ (18)

Let us now consider two cases.

Case 1

If m = 1.

Substituting Equations (15) and (16) into Equation (18) and equating the coefficients of $Y^i(\xi), (i = 0,1,2)$ on both sides of Equation (18), we have respectively

$$g(X)a_0(X) = a_1(X)[\frac{rX(\xi) + 2\omega\ell X^3(\xi)}{\ell c(\omega^2 - \ell^2)}],$$ (19)

$$\frac{da_o(X)}{dX} = g(X)a_1(X) + h(X)a_o(X),$$ (20)

$$\frac{da_1(X)}{dX} = h(X)a_1(X).$$ (21)

Since $a_i(X), \ (i = 0,1)$ are polynomials, then from Equation (21) we deduce that $a_1(X)$ is a constant and $h(X) = 0$. For simplicity we take $a_1(X) = 1$. Balancing the degrees of $g(X)$ and $a_0(X)$ we conclude that $\deg(g(X)) = 1$. Suppose that $g(X) = A_1X + B_o$, then we find

$$a_0(X) = \frac{1}{2}A_1X^2 + B_oX + A_o,$$ (22)

where A_1, B_o, A_o are constants to be determined. Substituting $a_0(X), a_1(X), g(X)$ into Equation (19) we get

$$[A_1X(\xi) + B_0][\frac{1}{2}A_1X^2(\xi) + B_0X(\xi) + A_0] - [\frac{rX(\xi) + 2\omega\ell X^3(\xi)}{\ell c(\omega^2 - \ell^2)}] = 0$$ (23)

Setting the coefficients of powers of $X(\xi)$ to zero, we obtain the following system of algebraic equations:

$$A_0 B_0 = 0,\ A_1 A_0 + B_0^2 = \frac{r}{\ell c(\omega^2 - \ell^2)},\ \frac{3}{2} A_1 B_0 = 0,\ A_1^2 = \frac{4\omega}{c(\omega^2 - \ell^2)} \quad (24)$$

On solving these algebraic equations, we have the results

$$A_1 = \pm 2\sqrt{\frac{\omega}{c(\omega^2 - \ell^2)}},\ B_0 = 0,\ A_0 = \frac{\pm r}{2\ell \sqrt{\omega c(\omega^2 - \ell^2)}} \quad (25)$$

From Equations (17), (22) and (25) we conclude that

$$Y(\xi) = -a_0(X) = \frac{\pm r}{2\ell \sqrt{\omega c(\omega^2 - \ell^2)}} \pm \sqrt{\frac{\omega}{c(\omega^2 - \ell^2)}} X^2(\xi) \quad (26)$$

and consequently we obtain the equation

$$X'(\xi) = \frac{\pm r}{2\ell \sqrt{\omega c(\omega^2 - \ell^2)}} \pm \sqrt{\frac{\omega}{c(\omega^2 - \ell^2)}} X^2(\xi) \quad (27)$$

Equation (27) is just the well-known Riccati equation. With reference to the article (Ma and Fuchssteiner, 1996) the authors proved that the Riccati equation $V' = \alpha_0 + \alpha_1 V + \alpha_2 V^2$, where $\alpha_0, \alpha_1, \alpha_2$ are constants such that $\alpha_2 \neq 0$ has the following solutions:

(i) If $\Delta = \alpha_1^2 - 4\alpha_0 \alpha_2 > 0$, then

$$V(\xi) = \begin{cases} \frac{-1}{2\alpha_2}[\alpha_1 + \sqrt{\Delta}\tanh(\frac{\sqrt{\Delta}}{2}\xi - \frac{\varepsilon \ln \xi_0}{2})] & if\ \xi_0 > 0 \\[3mm] \frac{-1}{2\alpha_2}[\alpha_1 + \sqrt{\Delta}\coth(\frac{\sqrt{\Delta}}{2}\xi - \frac{\varepsilon \ln(-\xi_0)}{2})] & if\ \xi_0 < 0 \\[3mm] \frac{-1}{2\alpha_2}[\alpha_1 + \varepsilon\sqrt{\Delta}] & if\ \xi_0 = 0 \end{cases} \quad (28)$$

(ii) If $\Delta = \alpha_1^2 - 4\alpha_0 \alpha_2 < 0$, then

$$V(\xi) = \begin{cases} \frac{-1}{2\alpha_2}[\alpha_1 - \sqrt{-\Delta}\tan(\frac{\sqrt{-\Delta}}{2}\xi + \xi_0)], \\[3mm] \frac{-1}{2\alpha_2}[\alpha_1 + \sqrt{-\Delta}\cot(\frac{\sqrt{-\Delta}}{2}\xi + \xi_0)]. \end{cases} \quad (29)$$

(iii) If $\Delta = \alpha_1^2 - 4\alpha_0 \alpha_2 = 0$, then

$$V(\xi) = \frac{-\alpha_1}{2\alpha_2} - \frac{1}{\alpha_2 \xi + \xi_0} \quad (30)$$

where ξ_0 is an arbitrary constant and $\varepsilon = \pm 1$.

With the aid of Equations (28) - (30) the solutions of Equation (11) have the forms:

(i) If $\dfrac{r}{\ell c(\omega^2 - \ell^2)} < 0,\ \dfrac{r}{\ell \omega} < 0$, we get

$$u_1(\xi) = \pm \sqrt{\frac{-r}{2\ell \omega}} \tanh[\sqrt{\frac{-r}{2\ell c(\omega^2 - \ell^2)}}\ \xi - \frac{\varepsilon \ln \xi_0}{2}] \quad if\ \xi_0 > 0$$

$$u_2(\xi) = \pm \sqrt{\frac{-r}{2\ell \omega}} \coth[\sqrt{\frac{-r}{2\ell c(\omega^2 - \ell^2)}}\ \xi - \frac{\varepsilon \ln(-\xi_0)}{2}] \quad if\ \xi_0 < 0$$

$$u_3(\xi) = \pm \frac{\varepsilon}{2}\sqrt{\frac{-r}{2\ell \omega}} \quad if\ \xi_0 = 0 \quad (31)$$

(ii) If $\dfrac{r}{\ell c(\omega^2 - \ell^2)} > 0,\ \dfrac{r}{\ell \omega} > 0$, we get

$$u_4(\xi) = \pm \sqrt{\frac{r}{2\ell \omega}} \tan[\sqrt{\frac{r}{2\ell c(\omega^2 - \ell^2)}}\ \xi + \xi_0]$$

$$u_5(\xi) = \pm \sqrt{\frac{r}{2\ell \omega}} \cot[\sqrt{\frac{r}{2\ell c(\omega^2 - \ell^2)}}\ \xi + \xi_0] \quad (32)$$

(iii) If $\dfrac{\omega}{c(\omega^2 - \ell^2)} > 0,\ r = 0$, we get

$$u_6(\xi) = \frac{\pm 1}{\sqrt{\dfrac{r}{c(\omega^2 - \ell^2)}}\ \xi \pm \xi_0}, \quad (33)$$

where ξ is given by Equation (12).

As a result, we find the periodic and solitary solutions of Equation (11) are new and when $\alpha = 1$ they are also different from the solutions found in (Alquran and Al-Khaled, 2012; Abazar, 2011).

Case 2

If m = 2.

In this case, Equations (17) and (18) respectively reduce to

$$Q[X(\xi),Y(\xi)] = a_o(X) + a_1(X)Y(\xi) + a_2(X)Y^2(\xi) = 0 \quad (34)$$

and

$$\frac{da_0(X)}{dX} + \frac{da_1(X)}{dX}Y(\xi) + \frac{da_2(X)}{dX}Y^2(\xi)]Y(\xi) + [a_1X + 2a_2(X)Y(\xi)][\frac{rX(\xi) + 2\omega\ell X^3(\xi)}{\ell c(\omega^2 - \ell^2)}]$$

$$= [g(X) + h(X)Y(\xi)][a_0X + a_1(X)Y(\xi) + a_2(X)Y^2(\xi)] \quad (35)$$

Equating the coefficient of powers of $Y(\xi)$ on both sides of Equation (35) we have

$$\frac{da_2(X)}{dX} = h(X)a_2(X) \quad (36)$$

$$\frac{da_1(X)}{dX} = g(X)a_2(X) + h(X)a_1(X) \quad (37)$$

$$\frac{da_0(X)}{dX} + 2a_2(X)[\frac{rX(\xi) + 2\omega\ell X^3(\xi)}{\ell c(\omega^2 - \ell^2)}] = g(X)a_1(X) + h(X)a_0(X) \quad (38)$$

$$g(X)a_0(X) = a_1(X)[\frac{rX(\xi) + 2\omega\ell X^3(\xi)}{\ell c(\omega^2 - \ell^2)}] \quad (39)$$

Since $a_i(X)$, $(i = 0,1,2)$ are polynomials, then from Equation (36) we deduce that $a_2(X)$ is constant and $h(X) = 0$.   For simplicity we take $a_2(X) = 1$. Balancing the degrees of $g(X)$ and $a_1(X)$ we conclude that deg $(g(X)) = 1$, and hence we get

$$g(X) = A_1X + B_o, \quad (40)$$

and $a_1(X) = \frac{1}{2}A_1X^2 + B_oX + A_o \quad (41)$

where A_1, B_o, A_o are constants to be determined, such that $A_1 \neq 0$. Now, Equation (38) becomes

$$\frac{da_0(X)}{dX} = [\frac{-2r}{\ell c(\omega^2 - \ell^2)} + A_1A_0 + B_0^2]X(\xi) + \frac{3}{2}A_1B_0X^2(\xi)$$

$$+ [\frac{-4\omega}{c(\omega^2 - \ell^2)} + \frac{1}{2}A_1^2]X^3(\xi) + A_0B_0 \quad (42)$$

and

$$a_0(X) = [\frac{-r}{\ell c(\omega^2 - \ell^2)} + \frac{1}{2}A_1A_0 + \frac{1}{2}B_0^2]X^2(\xi) + \frac{1}{2}A_1B_0X^3(\xi)$$

$$+ [\frac{-\omega}{c(\omega^2 - \ell^2)} + \frac{1}{8}A_1^2]X^4(\xi) + A_0B_0X(\xi) + d \quad (43)$$

where *d* is the constant of integration.
   Substituting Equations (40), (41) and (43) into Equation

(39) and equating the coefficients of powers of $X(\xi)$ we get

$$A_1 = \frac{\pm 4\omega}{\sqrt{\omega c(\omega^2 - \ell^2)}}, \; B_0 = 0, \; A_0 = \frac{\pm r}{\ell\sqrt{\omega c(\omega^2 - \ell^2)}}, \; d = \frac{r^2}{4\omega c\ell^2(\omega^2 - \ell^2)}$$

Consequently, we deduce that

$$a_0(X) = \frac{r}{\ell c(\omega^2 - \ell^2)}X^2(\xi) + \frac{\omega}{c(\omega^2 - \ell^2)}X^4(\xi) + \frac{r^2}{4\omega\ell^2 c(\omega^2 - \ell^2)} \quad (44)$$

and

$$a_1(X) = \pm\frac{2\omega}{\sqrt{\omega c(\omega^2 - \ell^2)}}X^2(\xi) \pm \frac{r}{\ell\sqrt{\omega c(\omega^2 - \ell^2)}} \quad (45)$$

Substituting Equations (44), (45) into Equation (34) we deduce after some reduction that

$$Y(\xi) = -\frac{1}{2}a_1(X) \quad (46)$$

and hence

$$X'(\xi) = \pm\frac{r}{2\ell\sqrt{\omega c(\omega^2 - \ell^2)}} \pm \frac{\omega}{\sqrt{\omega c(\omega^2 - \ell^2)}}X^2(\xi) \quad (47)$$

which has the same form Equation (27) and gives the same solutions (31) to (33). This shows that the two cases m=1 and m=2 give the same solutions. Comparing our results with the results ((Alquran and Al-Khaled, 2012; Abazar, 2011), it can be seen that our solutions are new.

Example 2. The nonlinear fractional Klein-Gordon-Zakharov equations

These equations are well- known (Thornhill and Haar, 1978; Dendy, 1990; Ebadi et al., 2010; Shang et al., 2008) and can be written in the following system:

$$D_{tt}^{2\alpha}u - u_{xx} + u + \beta_1 uv = 0,$$

$$D_{tt}^{2\alpha}v - v_{xx} - \beta_2(|u|)_{xx} = 0, \; 0 < \alpha \leq 1, \quad (48)$$

with $u(x,t)$ is a complex function and $v(x,t)$ is a real function, where β_1, β_2 are nonzero real parameters. This system describes the interaction of the Langmuir wave and the ion acoustic in a high frequency plasma. Using the wave variable

$$u(x,t)=\phi(x,t)\exp\left[i\left(kx+\frac{\omega t^{\alpha}}{\Gamma(1+\alpha)}+\xi_1\right)\right],\qquad(49)$$

where $\phi(x,t)$ is a real-valued function, k,ω are real constants to be determined and ξ_1 is an arbitrary constant. Then the system (48) is carried to the following PDE system:

$$D_{tt}^{2\alpha}\phi-\phi_{xx}+(k^2-\omega^2+1)\phi+\beta_1v\,\phi=0$$
$$\omega D_t^{\alpha}\phi-k\,\phi_x=0\qquad\qquad\qquad(50)$$
$$D_{tt}^{2\alpha}v-v_{xx}-\beta_2(\phi^2)_{xx}=0$$

Setting

$$v(x,t)=v(\xi),\quad \phi(x,t)=\phi(\xi),\quad \xi=\omega x+\frac{kt^{\alpha}}{\Gamma(1+\alpha)}+\xi_2\qquad(51)$$

where ξ_2 is an arbitrary constant, then we get

$$v(\xi)=\frac{\beta_2\omega^2\phi^2(\xi)}{(k^2-\omega^2)}+C,\qquad(52)$$

and

$$\phi''(\xi)+\ell_1\phi(\xi)+\ell_2\phi^3(\xi)=0\qquad(53)$$

where $\ell_1=\dfrac{(k^2-\omega^2+\beta_1C+1)}{(k^2-\omega^2)},\ \ell_2=\dfrac{\omega^2\beta_2\beta_1}{(k^2-\omega^2)^2}$, C is an

integration constant, and $k\neq\pm\omega$.
On using Equations (8) and (9), we deduce that Equation (53) is equivalent to the two dimensional autonomous system:

$$X'(\xi)=Y(\xi)\qquad\qquad(54)$$

$$Y'(\xi)=-\ell_1X(\xi)-\ell_2X^3(\xi)\qquad(55)$$

where $X(\xi)=\phi(\xi)$.
Now we consider the two cases.

Case 1

If m = 1.

Substituting Equation (54) and (55) into Equation (18) and equating the coefficients of $Y^i(\xi),(i=0,1,2)$ on

both sides of Equation (18), we have respectively.

$$g(X)a_0(X)=a_1(X)[-\ell_1X(\xi)-\ell_2X^3(\xi)],\quad(56)$$

$$\frac{da_o(X)}{dX}=g(X)a_1(X)+h(X)a_o(X),\qquad(57)$$

$$\frac{da_1(X)}{dX}=h(X)a_1(X).\qquad(58)$$

Since $a_i(X),\ (i=0,1)$ are polynomials we deduce that $h(X)=0$, $a_1(X)=1$ and deg $(g(X))=1$. Then we obtain

$$g(X)=A_1X+B_o,\qquad(59)$$

$$a_0(X)=\frac{1}{2}A_1X^2+B_oX+A_o\qquad(60)$$

Substituting $a_0(X),a_1(X),g(X)$ into Equation (56) we get

$$[A_1X(\xi)+B_0][\tfrac{1}{2}A_1^2X(\xi)+B_0X(\xi)+A_0]+\ell_1X(\xi)+\ell_2X^3(\xi)=0\qquad(61)$$

Setting the coefficients of powers of $X(\xi)$ to zero, we obtain

$$A_0B_0=0,\ A_1A_0+B_0^2=-\ell_1,\ \frac{3}{2}A_1B_0=0,\ A_1^2=-2\ell_2$$

On solving these algebraic equations, we have the results

$$A_1=\pm\sqrt{-2\ell_2},\ B_0=0,A_0=\pm\frac{\ell_1}{\sqrt{-2\ell_2}},\ \ell_2<0.$$

Now, we deduce that

$$X'(\xi)=\pm\frac{\ell_1}{\sqrt{-2\ell_2}}\mp\frac{1}{2}\sqrt{-2\ell_2}X^2(\xi)\qquad(62)$$

which represents the well-known Riccati equation. With the help of Equations (28) to (30) the solutions of the system (48) can be written in the forms:

(i) If $\ell_1<0$ and $\ell_2<0$ we get the hyperbolic and rational solutions

$$\begin{cases} u_1(\xi) = \pm\sqrt{-\ell_1/\ell_2} \ \tanh(\sqrt{\dfrac{\ell_1}{2}} \ \xi - \dfrac{\varepsilon \ln \xi_0}{2})\exp(i\,\xi), \ if \quad \xi_0 > 0 \\ \\ v_1(\xi) = \dfrac{-\beta_2\ell_1\omega^2}{\ell_2(k^2 - \omega^2)} \ \tanh^2(\sqrt{\dfrac{\ell_1}{2}} \ \xi - \dfrac{\varepsilon \ln \xi_0}{2}) + C, \ if \quad \xi_0 > 0 \end{cases}$$

(63)

$$\begin{cases} u_2(\xi) = \pm\sqrt{-\ell_1/\ell_2} \ \coth(\sqrt{\dfrac{\ell_1}{2}} \ \xi - \dfrac{\varepsilon \ln(-\xi_0)}{2})\exp(i\,\xi), \ if \quad \xi_0 < 0 \\ \\ v_2(\xi) = \dfrac{-\beta_2\ell_1\omega^2}{\ell_2(k^2 - \omega^2)} \ \coth^2(\sqrt{\dfrac{\ell_1}{2}} \ \xi - \dfrac{\varepsilon \ln(-\xi_0)}{2}) + C, \ if \quad \xi_0 < 0 \end{cases}$$

(64)

$$\begin{cases} u_3(\xi) = \pm\sqrt{-\ell_1/\ell_2} \ \exp(i\,\xi), \\ \\ V_3(\xi) = \dfrac{-\beta_2\ell_1\omega^2}{\ell_2(k^2 - \omega^2)} + C, \end{cases}$$

(65)

(ii) If $\ell_1 < 0$ and $\ell_2 < 0$ we get

$$\begin{cases} u_4(\xi) = \pm\sqrt{-\ell_1/\ell_2} \ \tan(\sqrt{\dfrac{-\ell_1}{2}} \ \xi + \xi_0)\exp(i\,\xi) \\ \\ v_4(\xi) = \dfrac{-\beta_2\ell_1\omega^2}{\ell_2(k^2 - \omega^2)} \ \tan^2(\sqrt{\dfrac{-\ell_1}{2}} \ \xi + \xi_0) + C, \end{cases}$$

(66)

$$\begin{cases} u_5(\xi) = \pm\sqrt{-\ell_1/\ell_2} \ \cot(\sqrt{\dfrac{-\ell_1}{2}} \ \xi + \xi_0)\exp(i\,\xi) \\ \\ v_5(\xi) = \dfrac{-\beta_2\ell_1\omega^2}{\ell_2(k^2 - \omega^2)} \ \cot^2(\sqrt{\dfrac{-\ell_1}{2}} \ \xi + \xi_0) + C, \end{cases}$$

(67)

(iii) If $\ell_1 = 0$ and $\ell_2 < 0$ we get the rational solutions

$$\begin{cases} u_6(\xi) = \dfrac{\pm 1}{[\sqrt{\dfrac{-\ell_2}{2}}\xi + \xi_0]}\exp(i\,\xi) \\ \\ v_6(\xi) = \dfrac{\beta_2\omega}{(k^2 - \omega^2)[\sqrt{\dfrac{-\ell_2}{2}}\xi + \xi_0]^2} + C \end{cases}$$

(68)

Case 2

If m = 2.

Substituting Equations (54) and (55) in to Equation (18)

and equating the coefficients of powers of $Y\,(\xi)$ on both sides of Equation (18), we get

$$\frac{da_2(X\,)}{dX} = h(X\,)a_2(X\,)$$

(69)

$$\frac{da_1(X\,)}{dX} = h(X\,)a_1(X\,) + g\,(X\,)a_2(X\,)$$

(70)

$$\frac{da_0(X\,)}{dX} + 2a_2(X\,)[-\ell_1X - \ell_2X^3] = g\,(X\,)a_1(X\,) + h(X\,)a_0(X\,)$$

(71)

$$g\,(X\,)a_0(X\,) = a_1(X\,)[-\ell_1X - \ell_2X^3].$$

(72)

Since $a_i\,(X\,), \ (i = 0,1,2)$ are polynomials, then from Equation (69) we deduce that $a_2(X\,)$ is a constant and $h(X\,) = 0$. For simplicity we take $a_2(X\,) = 1$. Balancing the degrees of $g\,(X\,)$ and $a_1(X\,)$ we conclude that $\deg\,(g\,(X\,)) = 1$, and hence we get

$$g\,(X\,) = A_1X + B_o,$$

(73)

$$a_1(X\,) = \frac{1}{2}A_1X^2 + B_oX + A_o,$$

(74)

where A_1, B_o, A_o are constants to be determined, such that $A_1 \neq 0$. Now, Equation (71) reduces to

$$\frac{da_0(X\,)}{dX} = [2\ell_1 + A_0A_1 + B_0^2]X + \frac{3}{2}A_1B_0X^2 + [2\ell_2 + \frac{1}{2}A_1^2]X^3$$

(75)

Integrating Equation (75) with respect to $X\,(\xi)$, we have

$$a_0(X\,) = [\ell_1 + \frac{1}{2}A_0A_1 + \frac{1}{2}B_0^2]X^2 + \frac{1}{2}A_1B_0X^3 + [\frac{\ell_2}{2} + \frac{1}{8}A_1^2]X^4 + d$$

(76)

where d is the constant of integration.

Substituting Equations (73), (74) and (76) into Equation (72) and equating the coefficients of powers of $X\,(\xi)$ we get

$$A_0 = \pm\ell_1\sqrt{\frac{-2}{\ell_2}}, \ A_1 = \pm 2\sqrt{-2\ell_2}, B_0 = 0, \ d = -\frac{\ell_1^2}{2\ell_2}$$

where $\ell_2 < 0$.

Consequently, we deduce that

$$a_0(X) = 3\ell_1 X^2(\xi) - \frac{1}{2}\ell_2 X^4(\xi) - \frac{\ell_1^2}{2\ell_2} \qquad (77)$$

and

$$a_1(X) = \pm\sqrt{-2\ell_2}\, X^2(\xi) \pm \ell_1\sqrt{\frac{-2}{\ell_2}}. \qquad (78)$$

Substituting Equations (77) and (78) into Equation (34) we deduce that

$$Y(\xi) = -\frac{1}{2}a_1(X) \pm \sqrt{-2\ell_1}X(\xi). \qquad (79)$$

Hence we conclude that

$$X'(\xi) = \pm\frac{\ell_1}{2}\sqrt{\frac{-2}{\ell_2}} \pm \sqrt{-2\ell_1}X(\xi) \pm \frac{1}{2}\sqrt{-2\ell_2}X^2(\xi), \qquad (80)$$

which represents the generalized Riccati equation. With the help of Equations (28) and (30) the solutions of the system (48) can be written in the forms:

(i) If $\ell_1 < 0$ and $\ell_2 < 0$ we get the hyperbolic and rational solutions

$$\begin{cases} u_7(\xi) = \sqrt{\ell_1/\ell_2}\ [1 \pm \sqrt{2}\tanh(\sqrt{-\ell_1}\ \xi - \frac{\varepsilon\ln\xi_0}{2})\exp(i\,\xi),\ if\quad \xi_0 > 0 \\ v_7(\xi) = \frac{\beta_2\ell_1\omega^2}{\ell_2(k^2-\omega^2)}[1 \pm \tanh(\sqrt{-\ell_1}\ \xi - \frac{\varepsilon\ln\xi_0}{2})]^2 + C,\ if\quad \xi_0 > 0 \end{cases} \quad (81)$$

$$\begin{cases} u_8(\xi) = \sqrt{\ell_1/\ell_2}\ [1 \pm \sqrt{2}\coth(\sqrt{-\ell_1}\ \xi - \frac{\varepsilon\ln(-\xi_0)}{2})\exp(i\,\xi),\ if\quad \xi_0 < 0 \\ v_8(\xi) = \frac{\beta_2\ell_1\omega^2}{\ell_2(k^2-\omega^2)}[1 \pm \coth(\sqrt{-\ell_1}\ \xi - \frac{\varepsilon\ln(-\xi_0)}{2})]^2 + C,\ if\quad \xi_0 < 0 \end{cases} \quad (82)$$

$$\begin{cases} u_9(\xi) = \sqrt{\ell_1/\ell_2}\ [1 \pm \varepsilon\sqrt{2}]\exp(i\,\xi), \\ v_9(\xi) = \frac{\beta_2\ell_1\omega^2}{\ell_2(k^2-\omega^2)}[1 \pm \varepsilon\sqrt{2})]^2 + C, \end{cases} \quad (83)$$

(ii) If $\ell_1 = 0$ and $\ell_2 < 0$
In this case we can show that $X(\xi)$ is complex. Since $X(\xi) = \phi(\xi)$, then $\phi(\xi)$ is complex. This contradicts (49) where $\phi(\xi)$ should be real. Thus this case is rejected.

(iii) If $\ell_1 = 0$ and $\ell_2 < 0$ we get the rational solutions

$$\begin{cases} u_{10}(\xi) = \dfrac{\pm 1}{[\sqrt{\frac{-\ell_2}{2}}\ \xi \pm \xi_0]}\exp(i\,\xi) \\ v_{10}(\xi) = \dfrac{\beta_2\ell_1\omega^2}{(k^2-\omega^2)[\sqrt{\frac{-\ell_2}{2}}\ \xi \pm \xi_0]^2} + C \end{cases} \qquad (84)$$

Comparing our results with the results in (Thornhill and Haar, 1978; Dendy, 1990; Ebadi et al., 2010; Shang et al., 2008) it can be seen that our results are new.

PHYSICAL EXPLANATIONS OF SOME OF OBTAINED SOLUTIONS

Here, we will present some graphs of our results to visualize the underlying mechanism of the original equations. Using the mathematical software Maple 15, we plot some of these obtained solutions which are shown in Figures 1 and 2.

The nonlinear fractional Zoomeron

The obtained solutions incorporate three types of explicit solutions namely, the hyperbolic, trigonometric and rational function solutions. From these explicit results, it easy to say that the solutions (31) are kink, singular and rational solutions respectively. While the solutions (32) are periodic solution and Equation (33) are the rational solutions. For more convenience the graphical representations of $u_1(x,t)$ and $u_4(x,t)$ of Equation (11) are shown in Figure 1.

The nonlinear fractional Klein-Gordan-Zakharov system of Equations (48)

The obtained solutions (63) are kink solutions, the solutions (64) are the singular, the solution (65) are rational. While the solutions (66) and (67) are periodic and the solutions (68) are rational. The graphical solutions (63) and (66) are shown in Figure 2.

CONCLUSIONS

The first integral method is applied successfully for finding the exact solutions of the nonlinear fractional Zoomeron equation and the nonlinear fractional Klein-Gordon- Zakharov system of equations. The performance of this method is reliable and effective and gives more solutions. Thus, we deduce that the proposed method can be extended to solve many systems of other areas such that physics, biology and chemistry. With the aid of the maple, we have assured the correctness of the
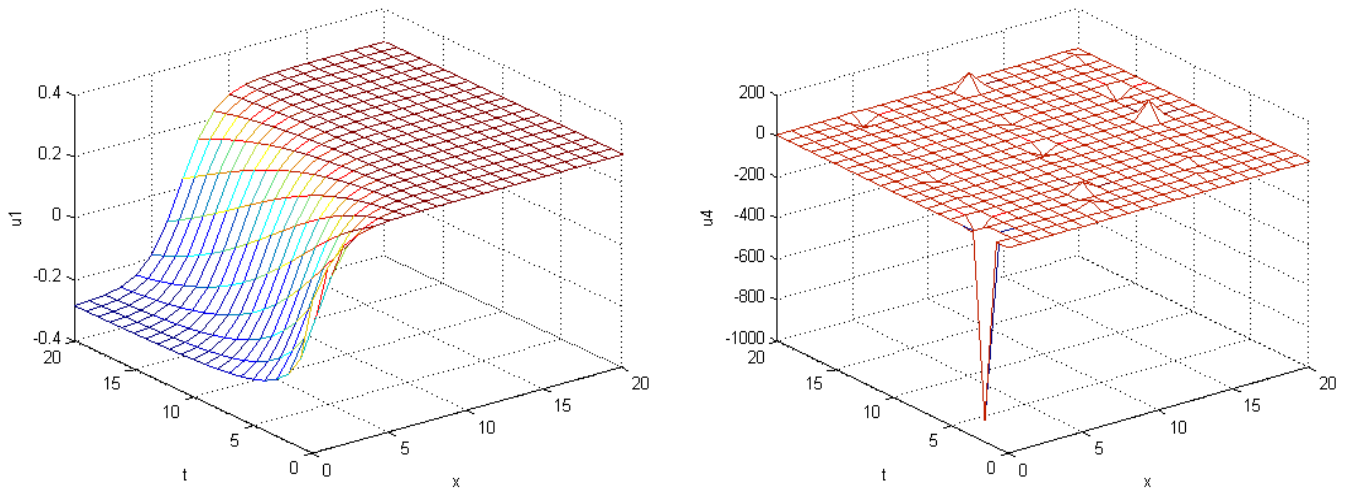
Figure 1. The plot of the solutions $u_1(\xi)$ and $u_4(\xi)$ of the nonlinear fractional Zoomeron equation.
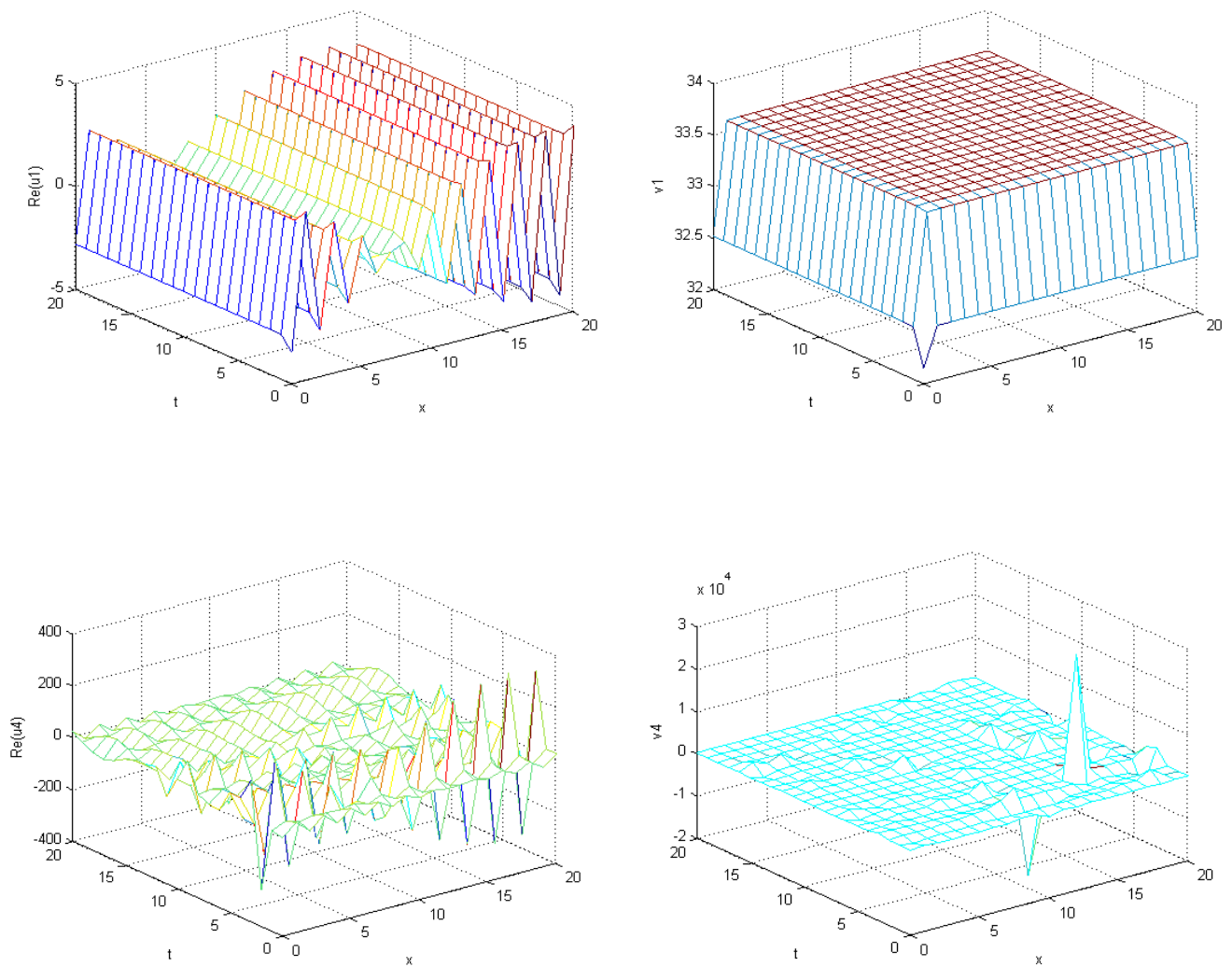

Figure 2. The plots of some of solutions of nonlinear fractional Klein-Gordon-Zakharov equations.

obtained solutions by putting them back to the original equations.

ACKNOWLEDGEMENT

The authors wish to thank the referees for their comments.

Conflict of Interests

The author(s) have not declared any conflict of interests.

REFERENCES

Abazar R (2011). The solitary wave soutions for Zoomeron equation, Appl. Math. Sci. 5:2943-2949.

Abbasbanby S, Shirzadi A (2010). Homotopy analysis method for multiple solutions of the fractional Sturm- Liouville problems, Numer. Algorithms 54:521-532. http://dx.doi.org/10.1007/s11075-009-9351-7

Alquran M, Al-Khaled K (2012). Mathematical methods for reliable treatment of (2+1)-dimentsional Zoomeron equation, Math. Sci. 6:11. http://dx.doi.org/10.1186/2251-7456-6-11

Baleanu D, Machado JAT, Carlo Cattani T, Baleanu MC, Yang XJ (2014). Local Fractional Variational Iteration and Decomposition Methods for Wave Equation on Cantor Sets within Local Fractional Operators, Abst. Appl. Anal. Article ID 535048, P. 6.

Barania G., Domairry G, Gorji M (2010). An approximation of the analytic solution of some nonlinear heat transfer in Fin and 3Ddiffusion equations using HAM, Numer. Methods in partial Differential Equations 26:1-13. http://dx.doi.org/10.1002/num.20404

Bourbak N (1972). Commutative Algebra, Paris Addison-Wesley.

Dendy RO (1990). Plasma Dynamics. Oxford University Press, Oxford. PMid:2339477

Ebadi G, Rashedi S, Bekir A (2010). New exact solutions to complex Klein-Gordon Schrodinger equations by the (G'/G) – expansion, Int. J. Nonlinear Sci. 10:475-483.

El-Sayed AMA, Rida SZ, Arafa AAM (2009). Exact solutions of fractional- order biological population model, Commun. Theor. Phys. (Beijing) 52:992-996. http://dx.doi.org/10.1088/0253-6102/52/6/04

Feng ZS, Roger K (2007). Traveling waves to Burgers-Korteweg-deVries-type equation with higher-order nonlinearties, J. Math. Anal. Appl. 328:1435-1450. http://dx.doi.org/10.1016/j.jmaa.2006.05.085

Feng ZS (2008). Travling wave behavior for a generalized fisher equation, Chaos Soltions and Fractals 38:481-488. http://dx.doi.org/10.1016/j.chaos.2006.11.031

Fouladi FE, Hosseinzadeh E, Barari A (2010). Highly nonlinear temperature- dependent Fin analysis by variational iteration method, Heat Transfer Res. 41:155-165. http://dx.doi.org/10.1615/HeatTransRes.v41.i2.40

Ganji Z, D.Ganji D, A.D.Ganji AD, Rostamian M (2010). Analytical solution of time-fractional Navier- Stokes equation in polar coordinate by homotopy perturbation method, Numer. Methods Partial Differential Equations 26:117-124. http://dx.doi.org/10.1002/num.20420

Gepreel KA (2011).The homotopy perturbation method applaied to the nonlinear fractional Kolmogorov-Petrovskii-Piskunov equation, Appl. Math.Lett. 24:1428-1434. http://dx.doi.org/10.1016/j.aml.2011.03.025

Gupta PK, Singh M (2011). Homotopy perturbation method for fractional Fornberg-Whitham equation, Comput. Math. Appl. 61:50-54. http://dx.doi.org/10.1016/j.camwa.2010.10.045

He JH (2012). Asymptotic Methods for Solitary Solutions and Compactons, Abstract and applied Analysis, Article ID 916793, P.130.

Inc M (2008). The approximate and exact solutions of the space- and time-fractional Burgers equations with initial conditions by variation iteration method, J. Math. Anal. Appl. 345:476-484. http://dx.doi.org/10.1016/j.jmaa.2008.04.007

Jumarie G (2006a). Lagrange characteristic method for solving a class of nonlinear partial differential equations of fractional order, Appl. Math. Lett. 19:873-880. http://dx.doi.org/10.1016/j.aml.2005.10.016

Jumarie G (2006b). Modified Riemann-Liouville derivative and fractional Taylor series of non-differentiable functions further results, Comput. Math. Appl. 51:1367-1376. http://dx.doi.org/10.1016/j.camwa.2006.02.001

Kilbas AA, Srivastava HM, Trujillo JJ (2006). Theory and Application of Fractional Differential Equations, Elsevier, San Diego.

Liu CF, Kong SS, Yuan SJ (2013). Reconsterucyive schemes for variational iteration method within Yang-Laplase transform with application to fractal heat conduction problem. Thermal Sci. 17: 715-721. http://dx.doi.org/10.2298/TSCI120826075L

Lu BHQ, Zhang HQ, Xie FD (2010). Traveling wave solutions of nonlinear partial equations by using the first integral method, Appl. Math. Comput. 216:1329-1336. http://dx.doi.org/10.1016/j.amc.2010.02.028

Ma WX, Fuchssteiner B (1996). Explicit and exact solutions to Kolmogorov-Petrovskii-Piskunov equation, Int. J. Nonli. Mech. 31:329-338. http://dx.doi.org/10.1016/0020-7462(95)00064-X

Miller KS, Ross BB (1993). An Introduction to the Fractional Differential Equations, Wiley, New York.

Podlubny I (1999). Fractional Differential, Acadmic press, San Diego.

Rashidi MM, Domairry G, Doosthosseini A, Dinarvand S (2009). Explicit approximate solution of the coupled KdV equations by using the homotopy analysis method, Int, J. Math. Anal. 12:581- 589.

Raslan HR (2008). The first integral method for solving some important nonlinear partial differential equations, Nonli. Dyn. 53:281-291. http://dx.doi.org/10.1007/s11071-007-9262-x

Safari M, Ganji DD, Moslemi M (2009). Application of He's variation alliteration method and Adomian's decomposition method to the fractional KdV- Burgers-Kuramoto equation, Comput. Math. Appl. 58:2091-2097. http://dx.doi.org/10.1016/j.camwa.2009.03.043

Shang YY, Huang YH, Yuan W (2008). New Exact traveling wave solutions for Klein-Gordon equations, Comput. Math. Appl. 56:1441-1450. http://dx.doi.org/10.1016/j.camwa.2007.10.033

Song LN, Zhang HQ (2009). Solving the fractional BBM-Burgers equation using the homotopy analysis method, Chaos Solutions Fractals 40:1616-1622. http://dx.doi.org/10.1016/j.chaos.2007.09.042

Taghizadeh T, Mirzazadeh M, Farahrooz F (2011). Exact solutions of the nonlinear Schrodinger equation by the first integral method, J. Math. Anal. Appl. 374:549-553. http://dx.doi.org/10.1016/j.jmaa.2010.08.050

Thornhill SG, Haar D (1978). Langmir turbulence and modulationl instability, Phys, Rep. 43:43-99. http://dx.doi.org/10.1016/0370-1573(78)90142-4

Wang SQ, Yong JU, Yang YJ, and Jassim HK, (2014). Local Fractional Function Decomposition Method for Solving Inhomogeneous Wave Equations with Local Fractional Derivative, Abst. Appl. Anal., Article ID 176395. P. 7.

Wu GC, Lee EWM (2010). Fractional variational iteration method and its application, Phys. Lett. A 374:2506-2509. http://dx.doi.org/10.1016/j.physleta.2010.04.034

Yang XJ, Baleanu D (2013). Fractal heat conduction problem solved by local fractional variation method, Therm. Sci. 17:625-628 http://dx.doi.org/10.2298/TSCI121124216Y

Yang XJ, Baleanu D, Zhong WP (2013). Approximate solutions for diffusion equations on Cantor space-time, Proc. Rom. Acad. Series A 14:27-133.

Yang XJ, Srivastava HM, He JH, Baleanu D (2013). Cantor-type cylindrical-coordinate method for differential equations with local fractional derivatives, Phys. Lett. A. 377:1996-1700. http://dx.doi.org/10.1016/j.physleta.2013.04.012

Zhao CG, Yang AM, Jafari H, Haghbin A (2014). The Yang-Laplace Transform for Solving the IVPs with Local Fractional Derivative, Abst. Appl. Anal. Article ID 386459, P. 5.

Zhang S, Zhang HQ (2001). Fractional sub-equation method and its applications to nonlinear fractional PDEs, Phys. Lett. A 375:1069-1073. http://dx.doi.org/10.1016/j.physleta.2011.01.029

Full Length Research Paper

Physicochemical characterization and inhibitive performance evaluation of *Commiphora kestingii* gum exudate in acidic medium

Paul Ocheje Ameh

Physical Chemistry Unit, Department of Chemistry, Nigeria Police Academy, Wudil, P. M. B. 3474, Kano State, Nigeria.

Gas chromatographic-mass spectrometry (GCMS), fourier transformed infra-red spectroscopy (FTIR) and physicochemical analysis of *Commiphora kestingii* gum have been carried out. The corrosion inhibition characteristics of *C. kestingii* (CK) gum on aluminium in sulphuric acid media were also investigated at 303 and 333K using gravimetric and scanning electron microscopic studies (SEM) method. The study revealed that the gum contains significant amount of Sucrose, Octadecanoic acid, Alpha camphorenal, Nerolidolisobutyrate, Diisopropenyl-1-methyl-1-vinyl cyclohexane, Abetic acid, Oleic acid, Verbenol, 2,6-dimethylhepta-1,5-diene, Naphthalene, Limonene, 7-hexadecenal and 10-methyl-8-tetradecen-1-ol acetate. Corrosion inhibition tests suggest that GS gum is a good inhibitor for the corrosion of Al in solution of H_2SO_4. The inhibition efficiency of this inhibitor increased with increasing temperature suggesting chemisorption mechanism. Also, the inhibition efficiency of these extract was found to increase in the presence of CK. Inhibition of Aluminium by *C. kestingii* gum occurred through synergistic adsorption of the various components of the gums hence the formation of multiple adsorption layer is proposed.

Key words: *Commiphora kestingii* gum, corrosion inhibitors, adsorption, aluminium.

INTRODUCTION

Aluminium has wider application ranging from all sorts packaging, vital in powerlines, the building and construction industry and common household objects (Hatch, 1984). The key features that lend aluminium to these uses are low density, ductility, electrical conductivity and strength in alloys. Aluminium has a natural corrosion protection from its oxide layer. However, the following factors may affect the stability of the aluminium oxide and thereby cause corrosion:

i. The oxide is not stable in acidic (pH < 4) or alkaline (pH

> 9) environments (Shimizu et al., 1991),
ii. Aggressive ions (chlorides, fluorides) may attack the oxide locally,
iii. Certain elements (Ga, Tl, In, Sn, Pb) may become incorporated in the oxide and destabilize it (Nisancioglu, 1992).

Several methods have been employed to improve and enhance the metal's life span, with the use of corrosion inhibitor being the most practical (Migahed and Nassar, 2008; Fouda and Ellithy, 2009). Corrosion inhibitors are

compounds or chemicals that react with metal surface and corrosion medium to protect the metal against corrosion. Most inhibitors are organic compounds synthesized from cheap raw materials. These non-toxic, benign, inexpensive, renewable and readily available alternative corrosion inhibitors have been found in different parts of plant extracts (Okafor et al., 2010; Ameh et al., 2012a, b; Eddy et al., 2012a, b).

Commiphora kestingii commonly called, Fula-fulfulde (fulani), Mbiji (Igbo), Nupe (Esha), Yoruba (Origbo) and Hausa (árár(r)ábií) belongs to the Burseraceas family. The tree usually approaches height of 2 to 5 m and is found mostly in rocks within the low altitudes dry woodland and bush of the savanna from Togo to Nigeria, and on to Ubangi-Shari. Notably, in most developing nations, the washed bark mixed with salt is applied to snakebites, and the fruit provides remedy for stomach ailments (Meer, 1980). The tree exudes a pale yellow liquid, which soon hardens to form yellowish red or reddish brown tears or masses that are then collected when the bark is incised (Meer, 1980).

The present study is aimed at elucidating the chemical structure of *C. kestingii* gum and investigating the corrosion inhibition and adsorption potentials of *C. kestingii* gum for the corrosion of Al in 0.1 M H_2SO_4 using gravimetric, SEM and fourier transformed infra-red spectroscopy (FTIR) techniques.

Collection of sample

Crude gum of *C. kestingii* (CK) was obtained as dried exudates from the parent trees grown at Samaru, Zaria in Sabon Gari LGA of Kaduna State. The outer bark of the tree was broken using a small axe. The cut was extended upward and downward to a significant depth and the gum formed was collected. The rate of formation of gum was found to depend on weather conditions. Gum formation was favoured by dry and retarded by cold or wet weather. The first set of gum was collected six weeks after tapping, while other samples were collected at an interval of two to three weeks. Gum droplets collected, were 2.0 to 7.5 cm in diameter. They dried and hardened on exposure to atmosphere.

Purification of gum

The crude sample of the gum consisted of a mixture of large and small modules and other impurities. These were hand sorted to remove fragments of bark and other visible impurities and then were spread out in the sun to dry for one to two weeks. The gum was then dissolved in cold distilled water and the solution strained through muslin, and centrifuged to obtain a small quantity of dense gel. The straw coloured supernatant liquor obtained was separated and acidified to a pH of 2 with dilute hydrochloric acid. Ethyl alcohol was added until it

was 80%. The gum precipitated out was removed by centrifugation at a rate of 2000 revolution per minute, washed with alcohol, ether and then dried in a desiccator.

Determination of physiochemical properties

Preliminary tests were performed to confirm the nature of the gum obtained. The test that were conducted are pH and solubility test.

Determination of pH

The pH of 2% w/v of the gum mucilage was determined using a Jenway pH meter (Model; 3505). The pH meter electrode was dipped into a buffer at a room temperature of 28°C after which it was removed, shaken a little to remove droplets of the buffer before immersion into the gum mucilage. The reading on the meter was recorded in triplicate measurements were made.

Determination of solubility in various solvents

The solubility of the gum was determined in cold and hot distilled water, acetone and chloroform. 10 mg sample of the studied gum exudate was added to 10 ml each of the solvents and left overnight. 5 ml of the clear supernatant was taken in small pre-weighed evaporating dishes and heated to dryness over a digital thermostatic water bath (Model. HHS, McDonald Scientific International). The weight of the dried residue with reference to the volume of the solutions was determined using a digital analytical balance (Model. XP-300, Denver instrument, USA) and expressed as the percentage solubility of the gum in the solvents (Carter, 2005).

MATERIALS AND METHODS

Corrosion studies

Aluminum alloy sheet of composition (wt. %, as determined by quantiometric method) Mn (1.28), Pb (0.064), Zn (0.006), Ti (0.029), Cu (0.81) and Si (0.381), Fe (0.57), and Al (96.65%) was used. The sheets were mechanically pressed cut into different coupons, each of dimension, 5 x 4 x 0.11 cm. Each coupon was degreased by washing with ethanol, cleaned with acetone and allowed to dry in the air before preservation in a desiccator. All reagents used for the study were analar grade and double distilled water was used for their preparation.

Gravimetric studies

The clean and dried previously weighed aluminum alloy coupon was completely immersed in 250 ml of the test solution in an open beaker. After every 24 h the corrosion product was withdrawn from the electrolyte, kept for 3 to 4 min in 70% nitric acid, washed thoroughly with distilled water and then dried and weighed. The

Table 1. Physiochemical properties of *Commiphora kestingii* gum.

Parameter	
Colour	Pale yellow
Odour	Odourless
Taste	Bland
pH (28°C)	5.2
Percentage yield (%w/w)	63.5
Solubility (%w/v)	
Cold water	14.00
Hot water	11.00
Acetone	2.00
Chloroform	0.00
Ethanol	2.00

experiment was repeated at 333K. In each case, the difference in weight for a period of 168 h was taken as the total weight loss. From the average weight loss (mean of three replicate analysis) results, the inhibition efficiency (%I) of the inhibitor, the degree of surface coverage (θ) and the corrosion rate of aluminum (CR) were calculated using 3.1 to 3.3, respectively (Ameh et al., 2012a).

$$\%I = \left(1 - \frac{W_1}{W_2}\right) \times 100 \tag{1}$$

$$\theta = \left(1 - \frac{W_1}{W_2}\right) \tag{2}$$

$$CR = \frac{\Delta W}{At} \tag{3}$$

where W_1 and W_2 are the weight losses (g) for aluminum in the presence and absence of the inhibitor, θ is the degree of surface coverage of the inhibitor, $\Delta W = W_2 - W_1$, A is the area of the aluminum coupon (in cm^2), t is the period of immersion (in hours) and ΔW is the weight loss of aluminum after time, t.

Scanning electron microscopic studies (SEM)

The aluminium samples immersed in sulphuric acid and in the inhibitor solution for a period of one day were removed, rinsed with double distilled water, dried and observed under a scanning electron microscope to examine the surface morphology. The surface morphology measurements of carbon steel were examined using JSM-5600 LV scanning electron microscope (SEM) of JEOL, Tokyo, Japan. The sample was mounted on a metal stub and sputtered with gold in order to make the sample conductive, and the images were taken at an accelerating voltage of 10 kV.

Chemical analysis of samples

FTIR analysis

FTIR analyses of the gum and that of the corrosion products (in the absence and presence of gum) were carried out using Scimadzu FTIR-8400S Fourier transform infra-red spectrophotometer. The sample was prepared in KBr and the analysis was done by scanning the sample through a wave number range of 400 to 4000 cm^{-1}.

Gas chromatography–mass spectrometry (GC-MS) analysis

GC-MS analysis was carried out on a GC Clarus 500 Perkin Elmer system. Interpretation on mass spectrum GC-MS was conducted using the database of National Institute Standard and Technology (NIST) Abuja, having more than 62,000 patterns. The spectrum of the unknown component was compared with the spectrum of the known components stored in the NIST library. The name, molecular weight and structure of the components of the test materials were ascertained. Concentrations of the identified compounds were determined through area and height normalization.

RESULTS AND DISCUSSION

Physiochemical parameters of *CK* gum

Table 1 presents physical (pH, colour, taste and percentage yield) and chemical properties (solubility in ethanol, acetone, chloroform, cold and hot water) of CK gum. The gum is odourless, pale yellow in colour (Figure 1) and has a characteristic bland taste. The gum has a pH of 5.2 indicating that it is mild acidic. It is soluble in both cold and hot water. However, its solubility tends to decrease with increase in temperature indicating that the gum is ionic. It has been found that the solubility of some ionic solutes tends to decrease due to the change of properties and structure of liquid water; the lower dielectric constant results in a less polar solvent. Also, an increase in temperature will increase the motion of dissolved particles by weakening the forces acting between the solute and solvent. This allows the dissolved gum to re-coagulate without dissolution hence the decrease in solubility (Ebbing and Gammon, 2005). CK gum is also found to be slightly soluble in ethanol and acetone. The solubility of the gum in ethanol may be due to the presence of polar and non-polar ends in ethanol,

Figure 1. Crushed crude dry and purified sample of *Commiphora kestingii* gum.

which makes it to dissolve some polar and non-polar compounds. On the other hand, aprotic solvents such as acetone tend to have large dipole moment (separation of partial positive and partial negative charges within the same molecule) and solvate positively charged species via their negative dipole. This probably explains why CK gum is soluble in acetone to some extent.

GC-MS study on CK gum

Figure 2 shows the GC-MS spectrum of CK gum. In Table 2, IUPAC names as well as concentrations of compounds identified from various lines in the spectrum are presented while their chemical structures are presented in Figure 3. The gas chromatographic-mass spectrometry (GCMS) spectrum of CK displayed 14 significant peaks. Since area under the chromatogram is proportional to concentration, area normalization was carried out and percentage concentrations of the respective chemical constituents were evaluated. The results obtained shows that the most abundant component of CK gum is sucrose (37.11%), followed by Octadecanoic acid (20.44%). The least abundant constituent was found to be 0.82% alpha camphorenal. Others constituents of the gum included nerolidolisobutyrate (1.72%), diisopropenyl-1-methyl-1-vinyl cyclohexane (13.10%), abetic acid (4.10%), oleic acid (2.14%), verbenol (1%), 2,6-dimethylhepta-1,5-diene

(6.11%), Naphthalene (1.40%), Limonene (2.34%), 7-hexadecenal (1.71%) and 10-methyl-8-tetradecen-1-ol acetate (6.20%). The molar mass and chemical formulas of these compounds are also presented in Table 2. Resolutions of each line in the spectrum of CK gum also revealed the occurrence of several fragmentation peaks for each fraction.

FTIR

Figure 4 presents the FTIR spectrum of CK gum. The spectrum displayed peaks due to C-H bend in phenyl ring (722.37 cm^{-1}), C-H stretch due to alkene at 981.8 cm^{-1}, C-O stretch vibrations due to carboxylic acid, alcohol, ether or esters at 1164.08 and 1239.31 cm^{-1}, C-H scissoring and bending vibrations at 1378.18 and 1465.95 cm^{-1}, C = O stretch due to aldehyde, ketone, carboxylic acid or esters at 1745.64 cm^{-1}, OH stretch due to carboxylic acid at 2853.78 and 2927.08 cm^{-1} and OH stretch due to alcohol or phenol at 3474.88 cm^{-1}.

Corrosion study

Effect of CK gum on the corrosion of Al in 0.1 M H$_2$SO$_4$

Figures 5 and 6 show the variation of weight loss with time for the corrosion of Al in 0.1 M H$_2$SO$_4$ containing
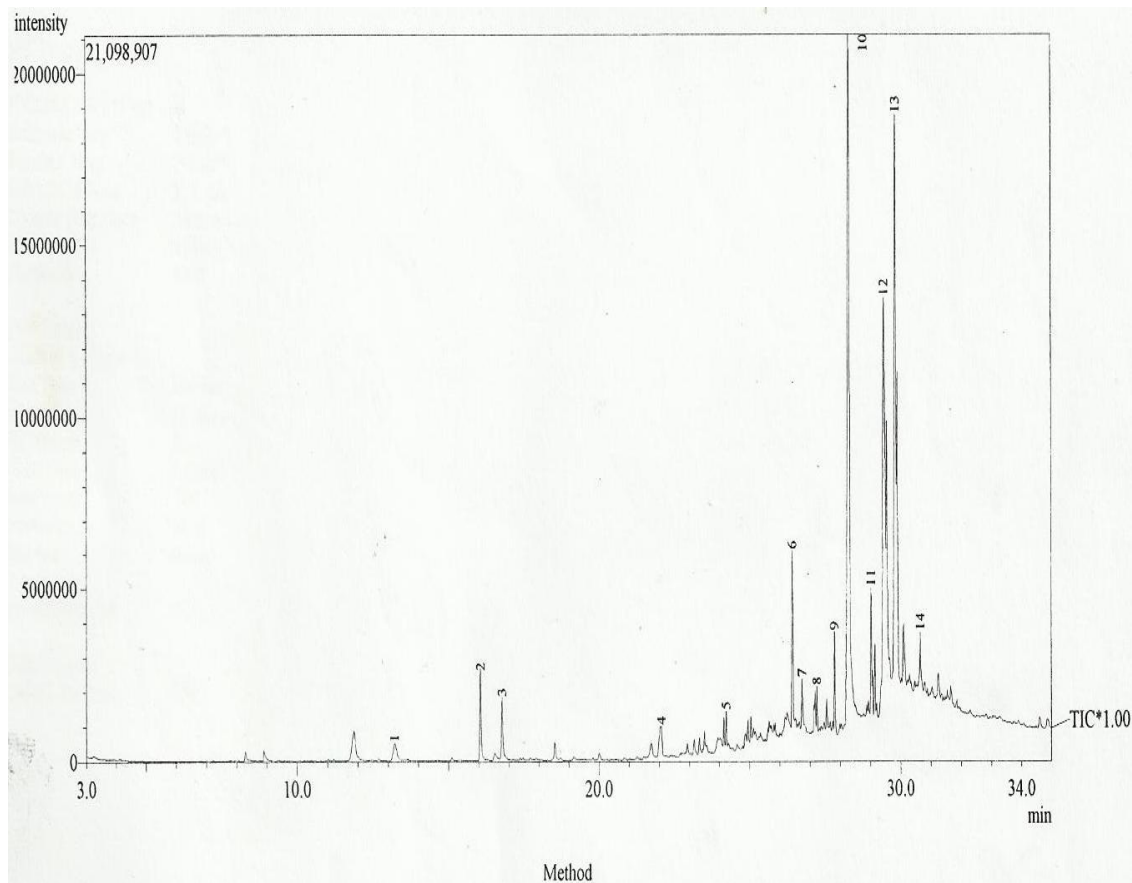
Figure 2. Chemical structures of compounds identified in the GC-MS spectrum of *Commiphora kestingii gum*.

various concentrations of CK gum at 303 and 333K. The figures revealed that the rate of corrosion of Al in solutions of H_2SO_4 increases with the period of contact but decreases with increase in the concentration of CK gum, indicating that CK gum is an adsorption inhibitor for the corrosion of aluminium. It has been found that for an adsorption inhibitor, the corrosion rate decreases with increase in the concentration of the inhibitor (Emregul and Hayvali, 2006).

Calculated values of corrosion rate of Al, inhibition efficiency of CK gum and degree of surface coverage calculated from Equations 1 to 3 are presented in Table 4. The results confirmed that the corrosion rate decreases with increase in temperature, while the inhibition efficiency increases with increase in temperature indicating chemical adsorption. For chemical adsorption mechanism, inhibition efficiency increases with temperature while for physical adsorption mechanism, inhibition efficiency of an inhibitor decreases with temperature (Ebenso et al., 2008). The inhibition efficiency of CK gum was found to range from 65.40 to 83.20% and from 74.90 to 83.22%, indicating that CK gum is a good inhibitor compare to values obtained for other inhibitors (Ameh et al., 2012b).

Kinetic study

Most corrosion reactions have been found to be first order and are consistent with the following equation (Ameh et al., 2012a)

$$-\log \text{(weight loss)} = k_1 t / 2.303 \tag{4}$$

where k_1 is the first order rate constant which is related to the half-life ($t_{1/2}$) through Equation 5:

$$t_{1/2} = 0.693/k_1 \tag{5}$$

Figures 7 and 8 depict plots for the variation of $-\log$ (weight loss) versus time for the corrosion of Al in solutions of H_2SO_4 containing various concentrations of CK gum at 303 and 333K, respectively. Kinetic parameters deduced from Equations 4 and 5 are presented in Table 5. The results obtained indicated that the corrosion of Al in solutions of H_2SO_4 obeys Equations 4 and 5. The half-lives in the presence of the CK gum are higher than those for the blanks at all temperature and concentrations of CK gum indicating that CK gum has the

Table 2. Characteristics of suggested compounds identified from GC-MS of *Commiphora kestingii* gum.

| Line no	C (%)	Compound	MF	MW	RT	Fragmentation peaks
1.	6.20	10-methyl-8-tetradecen-1-ol acetate	$C_{15}H_{28}O_2$	240	8.2	27(15%), 41(15%), 43(15%), 65(10%), 77(50%), 93(100%), 105(2%), 121(2%), 136(10 %)
2	1.81	n- Hexadecanoic acid	$C_{16}H_{32}O_2$	256	10.1	27(15%), 41(20%), 53(10%), 67(100%), 77(35%), 93(100%), 105(10%), 121(20%), 136(10%)
3	1.71	7-hexadecenal	$C_{16}H_{30}O$	238	35.2	41(80%), 55(90%), 71(78%), 85(50%), 98(40%), 121(40%), 135(20%), 141(10%)
4	2.34	Limonene	$C_{10}H_{16}$	136	9.8	27(40%), 39(60%), 53(45%), 68(100%), 79(40%), 93(65%), 107(20%), 121(20%), 136(25 %).
5	1.40	Naphthalene	$C_{20}H_{32}$	272	10.1	27(10%), 41(20%), 67(10%), 81(30%), 9(35%), 105(40%), 121(20%), 136(50%), 143(20%), 157(20%), 171(10%), 185(20%), 213(30%), 241(40%), 259 (50%)
6	6.11	2,6-dimethylhepta-1,5-diene	$C_{10}H_{16}$	136	10.5	27(20%), 41(100%), 53(20%), 69(80%), 77(25%), 93(100%), 107(8%), 121(10%), 136(5 %).
7	1.00	Verbenol	$C_{10}H_{16}O$	152	11.6	27(35%), 41(65%), 43(40%), 59(55%), 79(60%), 94(100%), 109(90%), 119(30%), 137(20%)
8	0.82	alpha-campholenal	$C_{10}H_{16}O$	152	12.0	27(15%), 39(20%), 55(20%), 67(25%), 81(20%), 93(55%), 108(100%), 119(5%), 137(2%), 152(2%)
9	2.14	Oleic acid	$C_{18}H_{34}O_2$	282	12.8	25(35%), 39(60%), 43(40%), 55(50%), 78(60%), 94(100%), 108(100%), 119(30%), 135(20 %)
10	37.11	Sucrose	$C_{12}H_{22}O_{11}$	152	14.3	25(20%), 39(40%), 43(20%), 67(20%), 78(100%), 94(50%), 108(40%), 119(30%), 134(20 %), 151(10%)
11	4.10	Abetic acid	$C_{20}H_{30}O_2$	302	14.8	25(10%), 39(32%), 55(35%), 69(20%), 81(30%), 83(55%), 108(100%), 119(20%), 134(10 %), 152(10%)
12	13.10	diisopropenyl-1-methyl-1vinylcyclohexane	$C_{15}H_{24}$	204	31.8	27(32%), 41(100%), 53(60%), 68(100%), 81(100%), 93(80%), 107(40%), 121(35%), 133(15 %), 147(20%), 161(15%), 189(15%).
13	20.44	Octadecanoic acid	$C_{18}H_{36}O_2$	284	33.2	27(12%), 39(18%), 43(38%), 59(100%), 81(50%), 93(70%), 107(40%), 121(30%), 135(22 %), 147(10%), 161(40%), 189(20%), 204(10%).
14	1.72	nerolidolisobutyrate	$C_{19}H_{32}O_2$	292	35.3	41(42%), 43 (100%), 69(25%), 71(50%), 93(30%), 107(10%), 121(40%), 127(5 %), 143(2%), 161(2%)
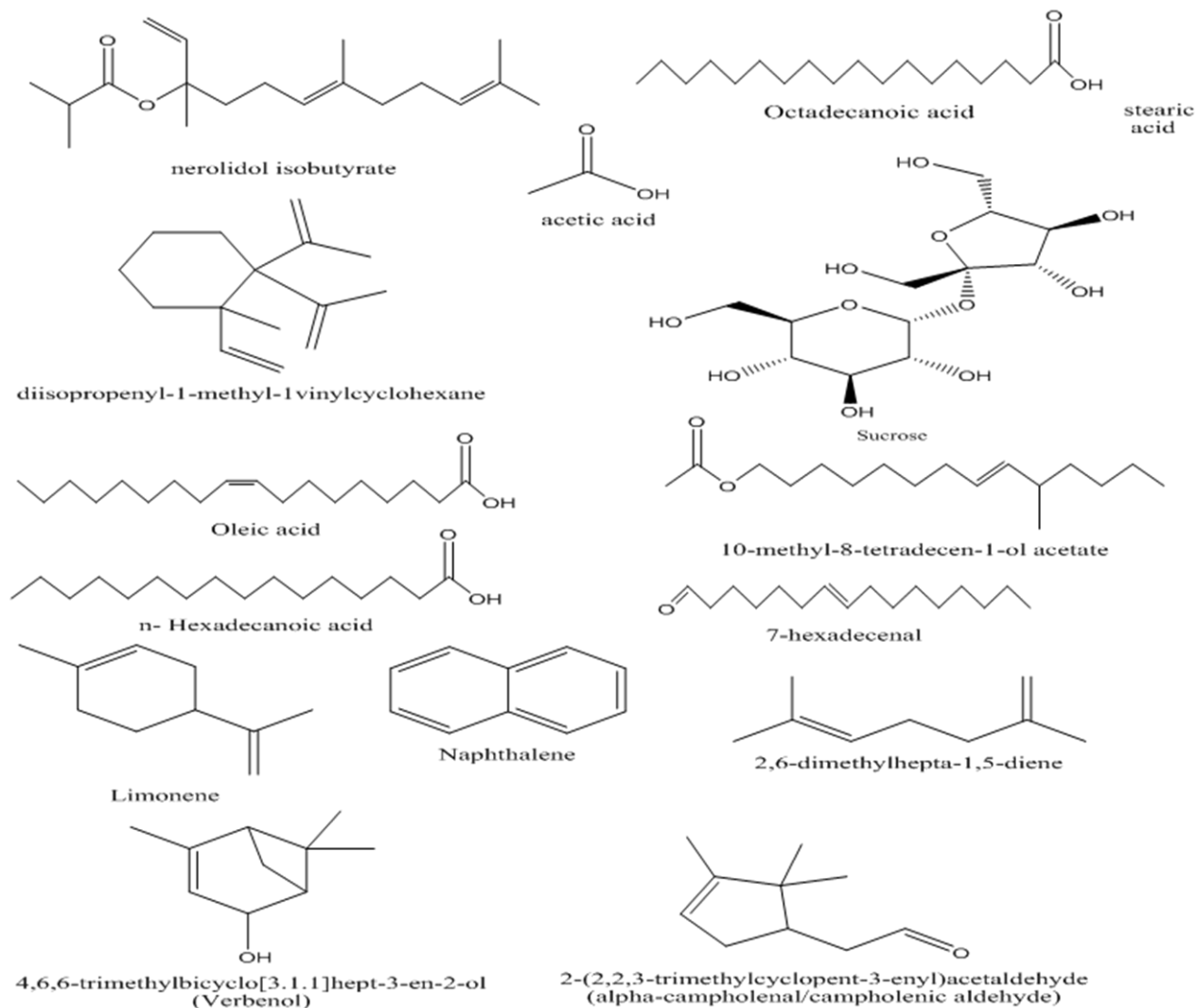
Figure 3. Chemical structures of compounds identified in GC-MS spectrum of CK gum.

tendency of extending the half-life of Al in solution of H_2SO_4, hence it is a good inhibitor.

The effect of temperature on the rate of corrosion of Al in solutions of H_2SO_4 containing various concentrations of CK gum was investigated using the Arrhenius equation, which can be written as follows (Ebenso, 2003a, b):

$$CR = A\exp(-E_a/RT) \tag{6}$$

where A is the pre-exponential factor, E_a is the activation energy, R is the gas constant and T is the temperature. By taking logarithm of Equations 6 and 7 was obtained:

$$\log(CR) = \log A - E_a/R \tag{7}$$

Between the temperature range of 303 (T_1) and 333 K (T_2) and the corresponding corrosion rates of CR_1 and CR_2, Equation 7 can be simplified to Equation 8 as follows:

$$\log \frac{CR_2}{CR_1} = \frac{E_a}{2.303R}\left(\frac{1}{T_1} - \frac{1}{T_2}\right) \tag{8}$$

In Table 6, calculated values of activation energy are recorded. The activation energies are relatively low when compared to the threshold value (80 kJ/mol) required for the mechanism of chemical adsorption. According to Oguzie (2006), lowered value of E_a in inhibited system compared to the blank as observed in the study (Table 6) is indicative of chemisorption possibly because some of the energy is used up in the chemical reaction. E_a tends to decrease in the presence of an inhibitor by decreasing the available reaction area.
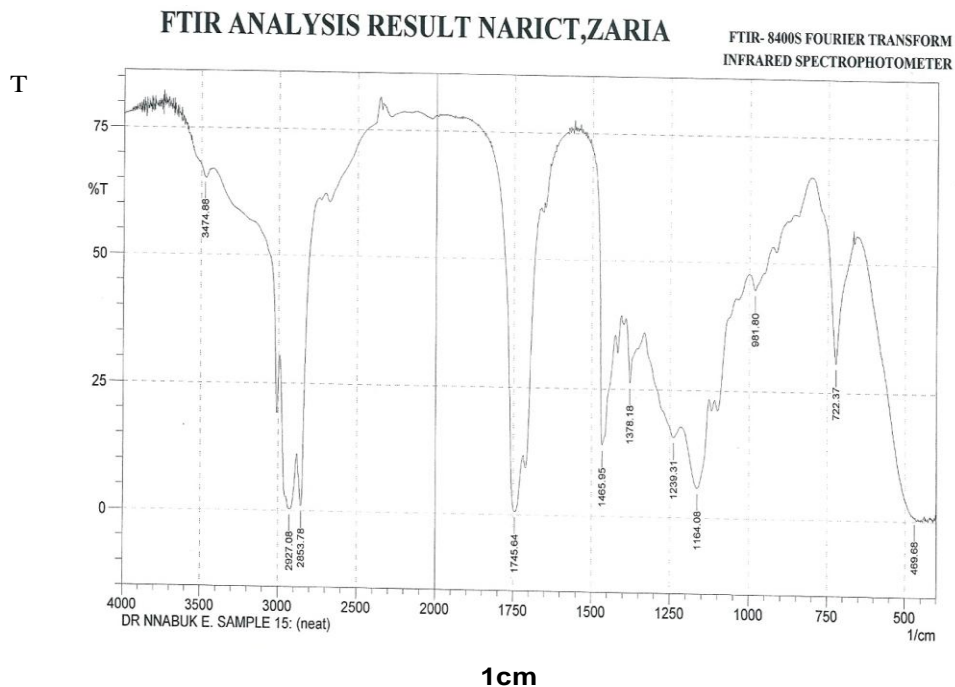
Figure 4. FTIR spectrum of *Commiphora kestingii* gum.

Figure 5. Variation of weight loss with time for the corrosion of Al in HCl containing various concentrations of *CK* gum at 303K.

It is also significant to note that E_a values tend to increase with increase in the concentration of CK gum indicating better adsorption strength with increasing concentration.

Thermodynamic/adsorption study

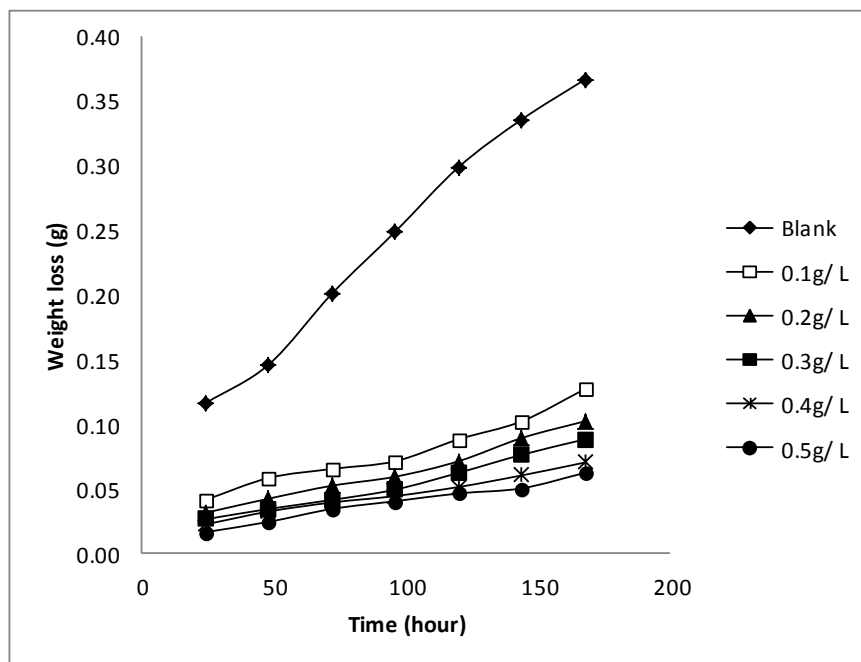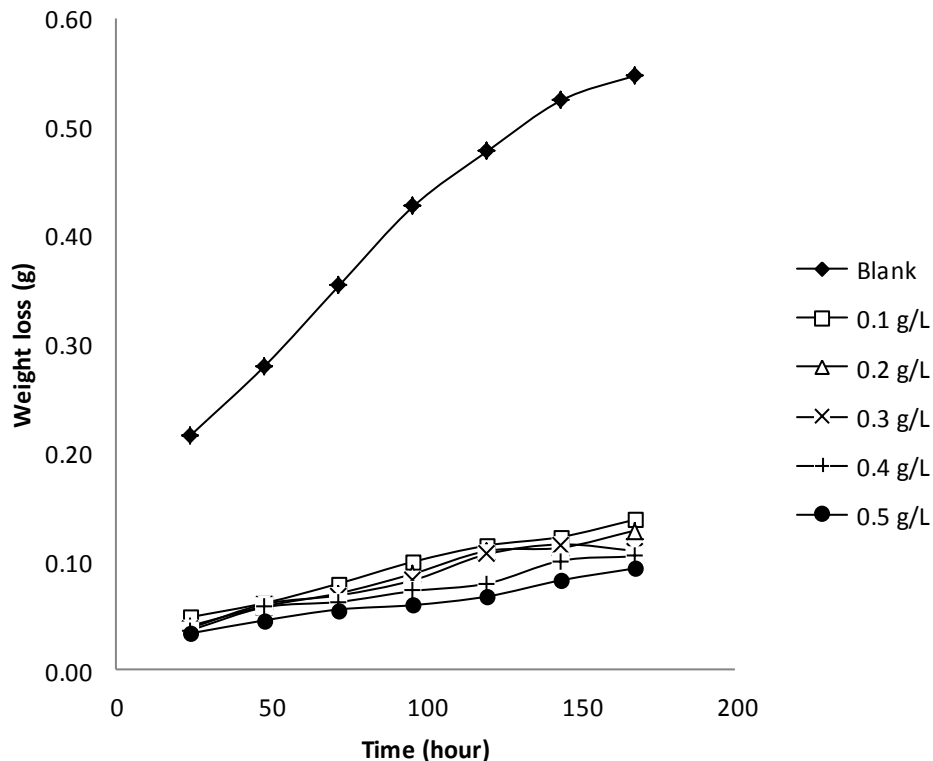The heat accompanying the adsorption of CK gum on

Figure 6. Variation of weight loss with time for the corrosion of Al in HCl containing various concentrations of *CK* gum at 333 K.

Table 3. Peaks and intensity of adsorption of FTIR by *CK* gum.

Peak	Intensity	Area	Assignments/functional groups
469.68	0.619	10.211	
722.37	30.649	39.968	C-H bend due to phenyl ring substitution
981.8	44.661	16.031	C-H stretch due to alkene
1164.08	5.805	84.851	C-O stretch due to carboxylic acid, alcohol, ether, and esters
1239.31	15.641	76.575	C-O stretch due to carboxylic acid, alcohol, ether, and esters
1378.18	26.289	18.176	C-H scissoring and bending due to alkane
1465.95	13.963	15.642	C-H scissoring and bending due to alkane
1745.64	0.593	42.869	C=O stretch due to aldehyde, ketones, carboxylic acid and esters
2853.78	0.957	86.542	OH stretch due to carboxylic acid
2927.08	0.321	47.798	OH stretch due to carboxylic acid
3474.88	65.27	5.111	OH stretch due to alcohol or phenol

Table 4. Corrosion rates for Al, inhibition efficiency and degree of surface coverage of *CK* gum in 0.1M H_2SO_4.

C (g/L)	CR (g/cm^3/h) at 303K	%I (303K)	θ (303K)	CR (g/cm^3/h) at 333 K	%I (333K)	θ (333K)
Blank	1.09×10^{-4}	-	-	1.63×10^{-4}	-	-
0.1	3.77×10^{-5}	65.40	0.654	4.10×10^{-5}	74.90	0.749
0.2	303×10^{-5}	72.30	0.723	3.80×10^{-5}	76.70	0.767
0.3	2.61×10^{-5}	76.10	0.761	3.24×10^{-5}	80.20	0.802
0.4	2.08×10^{-5}	81.00	0.810	3.09×10^{-5}	81.10	0.811
0.5	1.84×10^{-5}	83.20	0.832	2.76×10^{-5}	83.22	0.831

Figure 7. Variation of –log(weight loss) with time for the corrosion of Al in 0.1 M HCl containing various concentrations of CK gum at 303K.

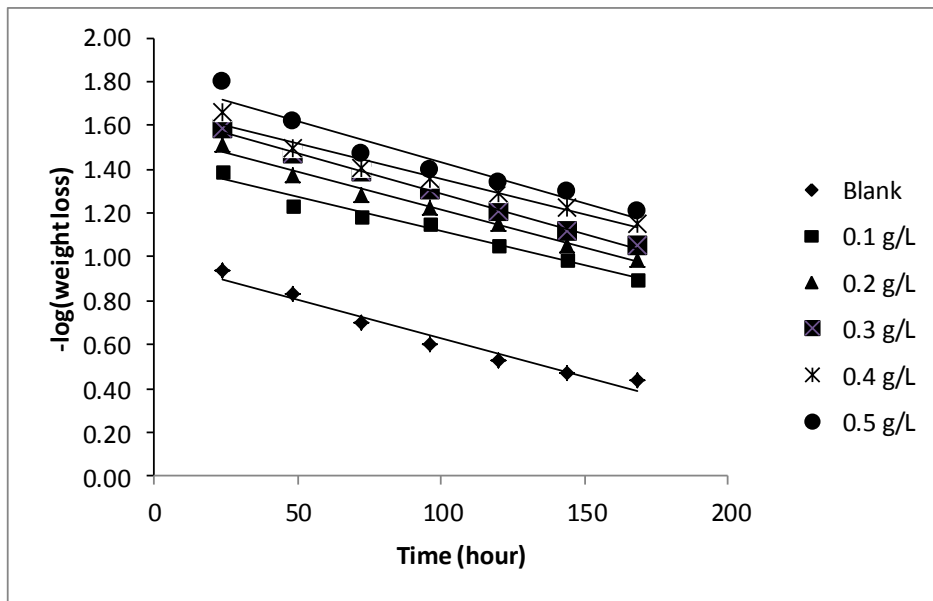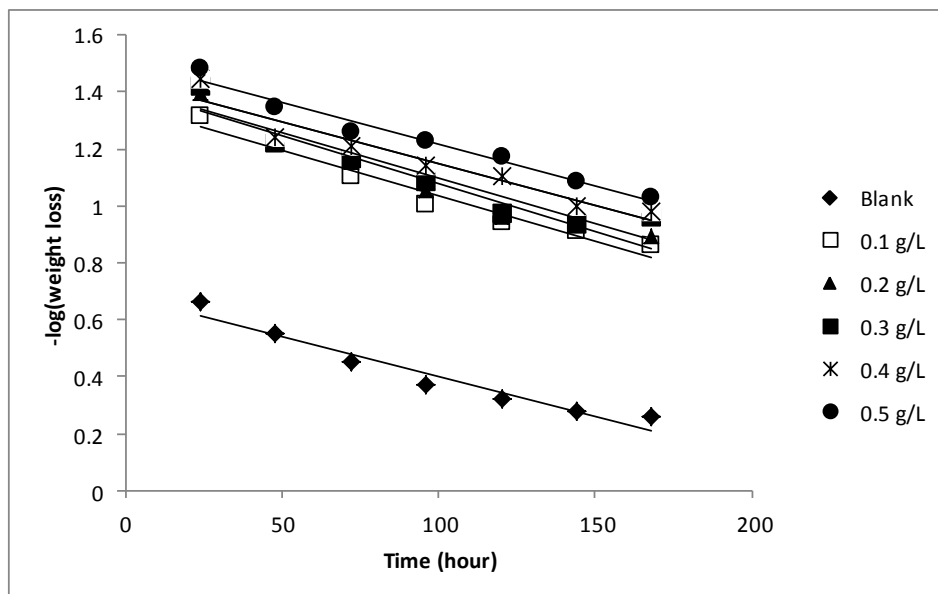**Figure 8.** Variation of –log(weight loss) with time for the corrosion of Al in 0.1 M HCl containing various concentrations of CK gum at 333K.

aluminum surface was calculated using the following equation (Eddy et al., 2012b):

$$Q_{ads} = 2.303R\left(\frac{\theta_2}{1-\theta_2} - \frac{\theta_1}{1-\theta_1}\right) \times \left(\frac{T_1 \, x \, T_2}{T_2 - T_1}\right) \quad (9)$$

Where Q_{ads} is the heat of adsorption, R is the universal gas constant, θ_2 and θ_1 are the degree of surface coverage at the temperatures T_1 (303K) and T_2 (333K), respectively. Calculated values of Q_{ads} are also recorded in Table 6. The results obtained reflect an endothermic process. Adsorption characteristics of a corrosion inhibitor can be simplified, using adsorption isotherms. In order to achieve this, the degrees of surface coverage at

Table 5. Kinetic parameters for the corrosion of Al in 0.1 M H_2SO_4 containing various concentrations of CK gum.

T (K)	C (g/L)	Slope	Intercept	k_1	R^2	$t_{1/2}$ (day)
303 K	Blank	-0.0036	0.986	0.008291	0.9634	1
	0.1	-0.0031	1.4282	0.007139	0.9764	2
	0.2	-0.0035	1.5612	0.008061	0.9883	2
	0.3	-0.0037	1.6571	0.008521	0.996	2
	0.4	-0.0032	1.6797	0.00737	0.9658	2
	0.5	-0.0038	1.8088	0.008751	0.9353	2
333 K	Blank	0.0028	0.6843	0.006448	0.9377	1
	0.1	0.0032	1.3563	0.00737	0.9583	2
	0.2	0.0034	1.4186	0.00783	0.94559	2
	0.3	0.0032	1.4147	0.00737	0.8920	2
	0.4	0.0029	1.4427	0.006679	0.9270	2
	0.5	0.0029	1.5094	0.006679	0.9700	2

Table 6. Activation energy and heat of adsorption of various concentrations of CK gum on Al surface.

C (g/L)	E_a (kJ/mol)	Q_{ads} (kJ/mol)
Blank	11.27	
0.1	2.35	52.83
0.2	6.34	32.93
0.3	6.35	41.85
0.4	11.08	1.34
0.5	11.15	3.46

various concentrations of the inhibitor were used to test for the fitness of Langmuir, Freudlich, Flory-Huggins, El awardy et al., Temkin and Frumkin adsorption isotherms. The tests indicated that Freundlich, Temkin and Flory-Huggins adsorption isotherms are applicable to the adsorption of CK gum on aluminum surface.

Expression of Flory-Huggins isotherm is given by Equation 10:

$$log\left(\frac{\theta}{c}\right) = logb + xlog(1-\theta) \tag{10}$$

where x is the number of inhibitor molecules occupying one site (or the number of water molecules replaced by one molecule of the inhibitor). Other parameters are as defined earlier. From Equation 10, a plot of $log(\theta/C)$ versus $log(1-\theta)$ should produce a straight line if the adsorption of the inhibitor follows Flory-Huggins isotherm. Flory-Huggins isotherm for the adsorption of CK gum is presented in Figure 9. Adsorption parameters deduced from the plots are presented in Table 7. From the results, it can be seen that R^2 values are very close to unity confirming the application of the Flory-Huggins adsorption parameters.

Temkin adsorption isotherm operates on the assumptions that relate the concentration of the inhibitor to the degree of surface coverage according to Equation 11:

$$exp(-2a\theta) = bC \tag{11}$$

where a is molecular interaction parameter; θ is degree of surface coverage, C is inhibitor concentration and b is equilibrium constant of the adsorption process. From the logarithm of both sides of Equation 11 and 12 is obtained

$$\theta = -\frac{lnK}{2a} - \frac{lnC}{2a} \tag{12}$$

From Equation 12, a plot of θ versus logC should give a straight line with slope equal to 2.303 x a/2 and intercept equal to 2.303 a logK/2 provided assumptions of Temkin isotherm are valid (Emregul et al., 2003, Emregul and Hayvali, 2006). Figure 10 presents Temkin isotherm for the adsorption of CK gum on aluminum surface while Temkin adsorption parameters are recorded in Table 7. The results indicated that the interaction parameters, 'a' are positive indicating the attractive behaviour of the inhibitor. The parameter tend to increase with increasing
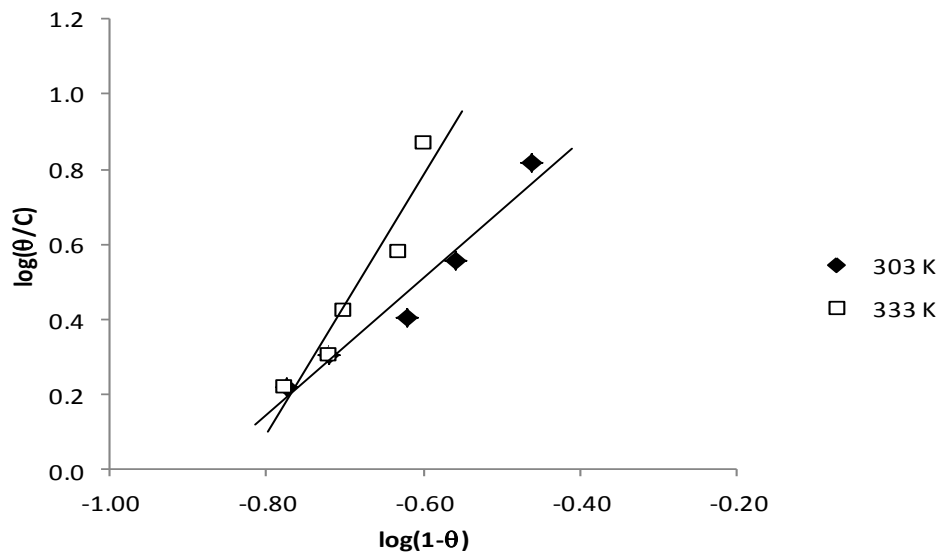
Figure 9. Flory-Huggins isotherm for the adsorption of CK gum on aluminum surface at 303 and 333K.

Table 7. Adsorption parameters for Flory-Huggins, Temkin and Freundlich adsorption isotherms.

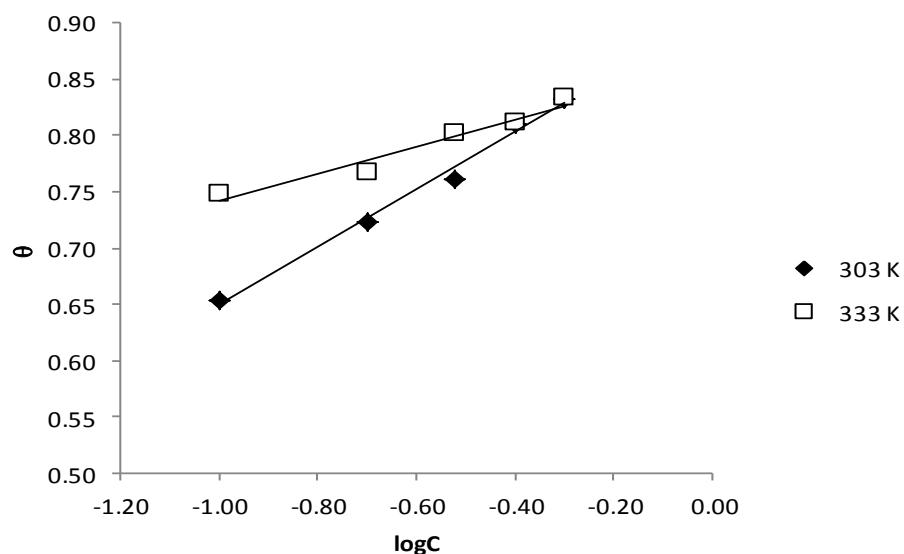| Isotherm	T (K)	Slope	Intercept	a or x	ΔG_{ads} (kJ/mol)	R^2
Florry-Huggins	303	0.2563	0.9057	0.26	-30.62	0.9901
	333	0.1208	0.8631	0.12	-51.57	0.9459
Temkin	303	1.8266	1.6068	4.49	-19.44	0.9584
	333	3.4301	2.8426	9.53	-26.61	0.9169
Freundlich	303	0.1508	1.965	6.63	-21.52	0.9946
	333	0.065	1.9365	15.38	-21.35	0.9552

Figure 10. Temkin isotherm for the adsorption of CK gum on aluminum surface at 303 and 333K.
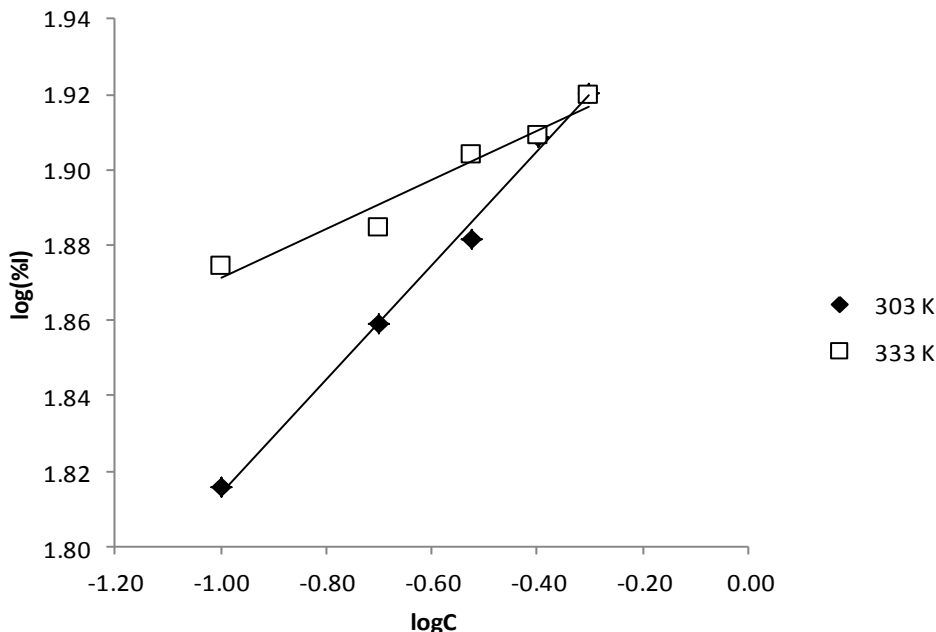
Figure 11. Freundlich isotherm for the adsorption of CK gum on aluminum surface at 303 and 333K.

temperature, which also indicate that the strength of adsorption increases with temperature and points toward chemisorption, which is expected to have chemical bond between the inhibitor and the metal surface.

Freudlich adsorption isotherm is an established isotherm for adsorption through physiosorption. The assumptions establishing the isotherm given in Equation 13 which simplifies to 14:

$$\frac{x}{m} = kC^{\frac{1}{n}} \tag{13}$$

$$log\left(\frac{x}{m}\right) = logk + \frac{1}{n}logC \tag{14}$$

The fraction x/m in Equation 14 is approximately the inhibition efficiency of a given inhibitor. Therefore from Equation 14, a plot of log[inhibition efficiency] versus logC should give a straight line if Freundlich isotherm is obeyed. Figure 11 shows Freundlich plots for the adsorption of CK gum on Al surface. Adsorption parameters deduced from the plots are also presented in Table 7.

Adsorption of organic adsorbate on the aluminum electrode surface is regarded as substitutional adsorption process between the organic molecule in the aqueous phase (Org_{ads}) and the water molecules adsorbed on the Al surface $(H_2O)_{ads}$:

$$xH_2O_{ads} + Org_{sol} \underset{\longleftarrow}{x\overrightarrow{Org_{ads}}} + H_2O_{sol} \tag{15}$$
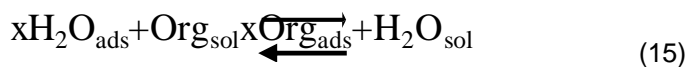
where x is the size ratio, that is, the number of water molecules replaced by one organic molecule.

From the Flory-Huggins adsorption isotherm, the value of x was computed to be 0.26 and 0.12 at 303 and 333K and the corresponding number of available adsorption site (n) computed from Freundlich adsorption isotherms were 6.63 and 15.38, respectively. These results show that the fraction of CK molecule adsorbed is temperature dependent, which point towards chemisorption, a mechanism whose extent of adsorption is expected to increase with increasing temperature.

Scanning electron microscopy (SEM) study

The scanning electron micrograph of the polished aluminium, uninhibited and inhibited aluminium in the presence of acidare shown in Figure 12a to c, respectively. It can be observed that there are distinct differences between the three SEM microphotographs. The SEM micrograph of aluminium surface (control) shows the smoothness of the metal surface implying the absence of any corrosion product formed on the metal surface.

The micrograph of the bared aluminum (Figure 12b) compared to the inhibited one (Figure 12c) shows that the former had suffered more severe corrosion than inhibitor protected one. The surface of the aluminum in the absence of the inhibitor was completely damaged after the exposure time while the CK–modified aluminium sheet was not so severely damaged. This means the
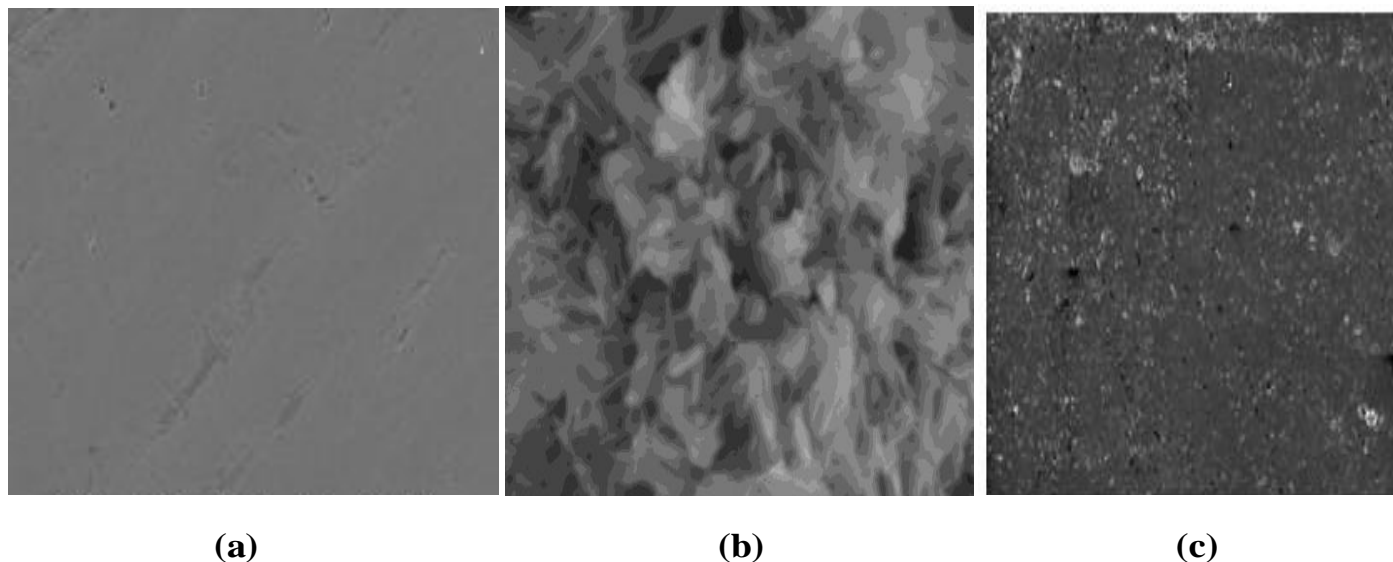
(a)   **(b)**   **(c)**

Figure 12. (a) Scanning electron micrograph of polished Al; (b) Scanning electron micrograph of Al in 0.1 M H_2SO_4 (without inhibitor); (c) Scanning electron micrograph of Al in 0.1 M H_2SO_4+ CK gum.

presence of CK gum can partially protect aluminum from corrosion.

Conclusion

This study shows that CK gum contains significant amount of Sucrose, Octadecanoic acid, Alpha camphorenal, Nerolidolisobutyrate, Diisopropenyl-1-methyl-1-vinyl cyclohexane, Abetic acid, Oleic acid, Verbenol, 2,6-dimethylhepta-1,5-diene, Naphthalene, Limonene, 7-hexadecenal and 10-methyl-8-tetradecen-1-ol acetate. Corrosion inhibition tests suggest that CK gum is a good inhibitor for the corrosion of Al in solution of H_2SO_4. The inhibition efficiency of this inhibitor increased with increasing temperature suggesting chemisorption mechanism. Also, the inhibition efficiency of these extract was found to increase in the presence of CK. Inhibition of aluminium by *C. kestingii* gum occurred through synergistic adsorption of the various components of the gums hence the formation of multiple adsorption layer is proposed.

Conflict of Interests

The author(s) have not declared any conflict of interests.

REFERENCES

Ameh PO, Magaji L, Salihu T (2012a). "Corrosion inhibition and adsorption behaviour for mild steel by *Ficus glumosa* gum in H_2SO_4 solution" Afr. J. Pure Appl. Chem. 6(7):100-106.

Ameh PO, Eddy NO, Gimba CE (2012b). Physiochemical and rheological studies on some natural polymers and their potentials as corrosion inhibitors. Published by Lambert Academic Publishing. UK.

Carter SJ (2005). Tutorial Pharmacy: Solution. Great Britain: Pitman Press: 1-8.

Ebenso EE (2003a). "Effect of halide on the corrosion inhibition of steel in H2SO4 using methyl red-Part1". Bull. Electrochem. 19(5):209-216.

Ebenso EE (2003b). "Synergistic effect of halides ions on the corrosion inhibition of aluminium in H_2SO_4 using 2-acetylphenothiazine". Mater. Chem. Phys. 79:58-70. http://dx.doi.org/10.1016/S0254-0584(02)00446-7

Ebenso EE, Eddy NO, Odiongenyi AO (2008). "Corrosion inhibitive properties and adsorption behaviour of ethanol extract of Piper guinensis as a green corrosion inhibitor for mild steel in H_2SO_4". Afr. J. Pure Appl. Chem. 4(11):107-115.

Eddy NO, Ameh PO, Gimba EC, Ebenso EE (2012a). "Chemical information from GCMS of Ficusplatyphylla gum and its corrosion inhibition potential for mild steel in 0.1 M HCl". Int. J. Electrochem. Sci. 7:5677–5691.

Eddy NO, Odiongenyi AO, Ameh PO Ebenso EE (2012b). "Corrosion inhibition potential of Daniella Oliverri gum exudate for mild steel in acidic medium". Int. J. Electrochem. Sci. 7:7425-7439.

Emregul KC, Hayvali M (2006). "Studies on the effect of a newly synthesized Schiff base compound from phenazone and vanillin on the corrosion of steel in 2M HCl". Corros. Sci. 48:797-812. http://dx.doi.org/10.1016/j.corsci.2005.03.001

Emregul KC, Kurtaran CR, Atakol O (2003). An investigation of chloride-substituted Schiff bases as corrosion inhibitors form steel. J. Corros. Sci. 45:2803-2817. http://dx.doi.org/10.1016/S0010-938X(03)00103-3

Fouda AS, Ellithy AS (2009). "Inhibition effect of 4-phenylthiazole derivatives on corrosion of 304L stainless steel in HCl solution". Corros. Sci. 51:868–875. http://dx.doi.org/10.1016/j.corsci.2009.01.011

Hatch JE (1984). Aluminium - Properties and physical metallurgy, ASM, Ohio: 242-264.

Meer W (1980). In hand book of water soluble Gums and Resins, Ed. R. L. Davidson, Mc Graw-Hill, New York. 8(1-8):24.

Migahed MA, Nassar IF (2008). "Corrosion inhibition of tubing steel during acidization of oil and gas wells". Electrochim. Acta. 53:2877–2882. http://dx.doi.org/10.1016/j.electacta.2007.10.070

Nisancioglu K (1992). Corrosion of aluminium alloys. Proceedings of

ICAA3, Trondheim, NTH and SINTEF. 3:239-259.

Oguzie EE (2006). "Adsorption and corrosion inhibitive properties of Azadirachta indica in acid solutions". Pigment Resin Technol. 35(6):334-340. http://dx.doi.org/10.1108/03699420610711335

Okafor PC, Ebenso EE, Ekpe UJ (2010). "*Azadirachta indica* extracts as corrosion inhibitor for mild steel in acid medium". Int. J. Electrochem. Sci. 5:973–998.

Shimizu K, Furneaux RC, Thompson GE, Wood GC, Gotoh A, Kobayashi K (1991). On the nature of "easy paths" for the diffusion of oxygen in thermal oxide films on aluminium, Oxidation of aluminium, 35(5/6):427-439.

Full Length Research Paper

An electrostatic lens system for the deceleration of high intensity heavy ion beams

F. W. Abdelsalam, M. M. Abdelrahman* and B. A. Soliman

Accelerators and Ion Sources Department, Nuclear Research Center, Atomic Energy Authority P. O. Box: 13759Inchas, Atomic Energy, Cairo, Egypt.

This work focuses on the design and implementation of an electrostatic lens system to produce high-intensity, low-energy ion beams, by means of numerical simulation of the beam trajectories (SIMION 7). The lens design was optimized using the simulation data obtained with a performance characteristics of the electrostatic lens system. This lens system maintains good beam focal quality for the deceleration of heavy ion beams of argon ions of with space charge of 10 mA. The beam emittance and beam diameter as a function of the gap width for a decel voltage of 45 kv of a deceleration lens system for a singly charged argon ion trajectories were investigated. A gap width of 5 mm and a tube diameter of 26 mm were found to be the minimum values. Also, a minimum of 24 mm of inner tube diameter was obtained for the relation between the inner tube diameter and the beam diameter. Beam emittance and beam diameter as a function of the focusing points for a decel voltage of 45 kv of a deceleration lens system for a singly charged argon ion trajectories was studied. A minimum of 455 mm was obtained at the outer exit of the deceleration lens system. While for the beam diameter, a minimum of 460 mm was deduced. It was found also that, a minimum of $V_{decel} = 43$ kV, deceleration voltage was obtained for the relation between the deceleration voltage and beam emittance. Also, a minimum of $V_{decel} = 49$ kV was found for the relation between the deceleration voltage and beam diameter.

Key words: Deceleration lens system and decel voltage, SIMION computer program, Beam emittance and beam radius.

INTRODUCTION

High-current ion beams are widely used for basic research and high technology applications, including for example, heavy ion fusion research, high current linear accelerators, spacecraft control systems, high dose ion implantation for material surface modification, and for surface cleaning and activation prior to film deposition (Goncharov, 2013). The advent of sophisticated computational techniques for simulating the actions of electric and magnetic fields on the motions of charged-particle beams under their influence has greatly facilitated

the design of low-aberration systems for use in ion acceleration and transport. These codes have been employed to design a variety of beam transport components, including lenses, magnets, steerers, deceleration/acceleration electrode systems, etc., and to simulate ion extraction from solid and plasma emitters. Among the computer codes for simulating the extraction of space-charge-dominated ion beams from plasma ion sources are those described according to Whealton and Whitson (1980), Whealton et al. (1988), Boers (1993), Spadtke (1983) and Becker and Herrmannsfeldt (1992). Electrostatic cylinder lenses are widely used to control beams of charged particles with different energies and directions in experiments covering many applications including electron spectroscopy, surface science and mass spectroscopy (Sise et al., 2007; 2005), and find use in focused ion beam systems, where they are more effective than magnetic lenses.

Electrostatic lenses usually consist of simple electrodes which are easy to manufacture and align. The major manufacturating problems are electric breakdown and the accumulation of charges on the insulating surfaces. The properties of the lenses comprising a pair of symmetrically arranged cylinders depend on a large number of parameters: the electrode voltage ratios, cylinder sizes and the gap between the electrodes. The field of electron and ion optics is based on the analogy between geometrical light optics and the motion of charged particles in electromagnetic fields. The aim is to concentrate as many particles in as small a volume as possible. The optical properties of electrostatic lenses are fixed by the voltage ratios. The focusing of charged particles with an electrostatic field can be achieved by devices consisting of a sequence of the accelerating electrodes with cylindrical symmetry which have lens – like properties. Recently, a heavy ion injector was installed at the Accelerators and Ion Sources Department, Nuclear Research Center, the Atomic Energy Authority (A.E.A), Egypt (Abdelrahman, 2009). The system is intended for use in isotope separators and ion implantation, as well as for research in the physics and technology of ion sources and surface physics. It is complete with power supply, control, vacuum and cooling system. This source (Nikiforov et al., 1996; Wielunski et al., 2004) was supplied by Efremov Research Institute of Electro Physical Apparatus, Saint Petersburg, Russia.

In the source, the ions are generated through crossed electric and magnetic fields discharge plasmas. The discharge is formed between the thermo emission core cathode and cylindrical anode surrounding it. The electrons emitted by the hot cathode have high ionization efficiency. The ions are extracted from the discharge region through an emission slit in the anode. The system uses an acceleration/deceleration scheme to avoid compensating electrons being accelerated back into the source, thus destroying its rear side and leaving the ion beam uncompensated. The main beam extraction

characteristics of this Freeman type ion source system were investigated with the SIMION computer program version 7, using singly charged argon ions with and without space charge (Abdelrahman and Abdelsalam, 2011).

It is the intent of this paper to discuss the computer beam optical properties for the deceleration lens system used to decelerate an ion beam extracted from a Freeman type ion source. Design and performance characteristics of the electrostatic lens system which maintains good beam focal quality for the deceleration of heavy ion beams of argon ions of space charge of 10 mA, are described.

CONSTRUCTION OF THE ION SOURCE

Ions of various elements are generated in this version of a Freeman type ion source (Aitken, 2004) and accelerated in a four electrode acceleration/deceleration extraction system to obtain energies of up to 50 keV. The ion source and the accelerating/decelerating system are constructed as a single unit mounted around the vacuum chamber of the system.

It consists of a thermoemission tungsten cathode rod with 2mm diameter, fixed inside a molybdenum anode by boron nitride insulators. The anode has an emission slit 40 mm in length and 0.5 – 2 mm wide, which is formed by two replaceable molybdenum plates mounted between the anode and the emission electrode, where the distance between the cathode and the exit slit is equal to 3.7 mm. An auxiliary magnetic field of 100 gauss is maintained parallel to the axis of the cathode. The anode contains three holes for feeding with gas, liquid or solid materials. A schematic diagram of this ion source system is shown in Figure 1.

EMITTANCE OF AN ION BEAM

A charged particle beam is a group of particles possessing about the same kinetic energy and moving in about the same direction. The high kinetic energies and good directionality of charged particles in beams make them useful for various applications, such as, beam lithography for micro circuits, thin film technology, radiation processing of materials, and free electron lasers (Jr. Humphries, 1990). Beams extracted from different types of ion sources have to be transmitted without any loss. It is very important that the particles striking the target should have the parameters required for the target application. For beam transmission without loss of particles, the cross section of the beam must not exceed a given maximum value of a well defined point. To achieve this we introduce a quantity, the emittance (El-saftawy, 2013) which is important for high quality beams and which is defined by the product of the width and the
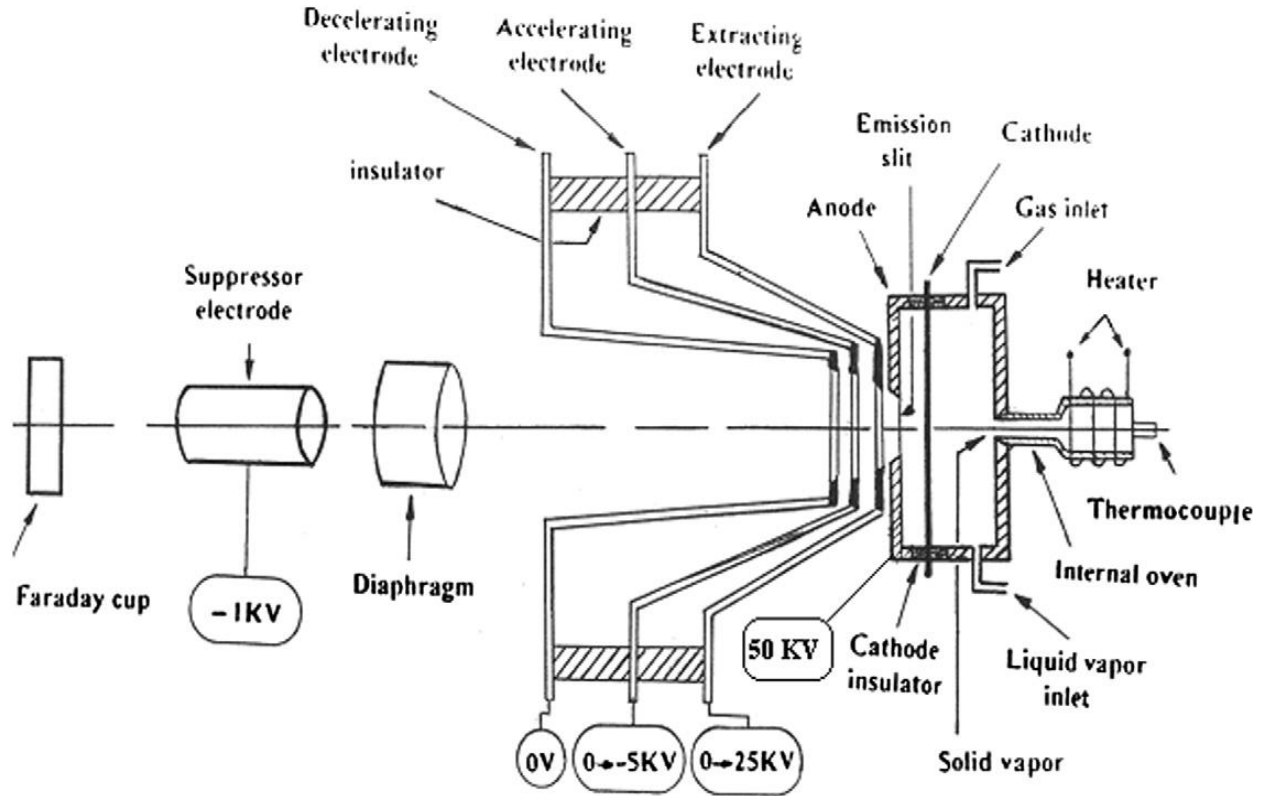
Figure 1. Schematic of the Freeman type ion source.

transverse velocity spread of the beam (region of phase space occupied by beam). If the beam is densely packed, then the emittance is said to be low and if it is somewhat spread out, it possesses high emittance (Masood et al., 2008). Any ion beam can be described in a six dimensional phase space (x, y, z, p_x, p_y, p_z), where (x, y, z) represents the position and (p_x, p_y, p_z) the momentum components of the ions. The emittance of the beam, which must be invariant and independent of any electrostatic or magnetic fields through which the beam passes, is subject to Liouville's theorem (Forrester, 1988), which states that the motion of charged particles under the action of conservative fields is such that the local number density in six dimensional phase space is a conserved quantity. If a group of ions or electrons is accelerated through the same potential difference and travelling with small angles relative to the z direction, we can say that they have a very small spread in z directed velocities and that this spread is invariant. Then the phase space (x, y, p_x, p_y) should be an invariant of the beam. For a beam with cylindrical symmetry, it implies that the two-dimensional area with coordinates (r, p_r) should be an invariant. At a certain position on the z axis (momentum component p_z approximately equals the total particle momentum *P*), we consider ions which pass through (x, y) related to r, and if cylindrical symmetry can

be assumed (Abdelrahman and Zakhary, 2009) then:

$$x' = \frac{p_x}{p_z} = \frac{p_x}{p}, y' = \frac{p_y}{p}, r' = \frac{p_r}{p} \tag{1}$$

Then,

$$\varepsilon_x = \frac{1}{\pi} A(x, x'), \varepsilon_y = \frac{1}{\pi} A(y, y'), \varepsilon_r = \frac{1}{\pi} A(r, r') \tag{2}$$

where ε_x , ε_y and ε_r are the transverse emittance or simply emittance in the (x-x'), (y-y') and (r-r') planes respectively. The values A (x, x'), A (y, y') and A (r, r') represent two dimensional phase space areas and remain constant along drift region (Figure 2).

The emittance is related to another property of accelerators or charged particle system namely the acceptance, sometimes called admittance. Acceptance is defined as the maximum emittance that a beam transport or analyzing system is able to transmit without flux loss. This is the size of the chamber transformed into phase space and does not suffer from the ambiguities of the definition of beam emittance. To get good performance of an ion beam transport system, the emittance should be much smaller than the acceptance (Lee, 1999). Figure 3
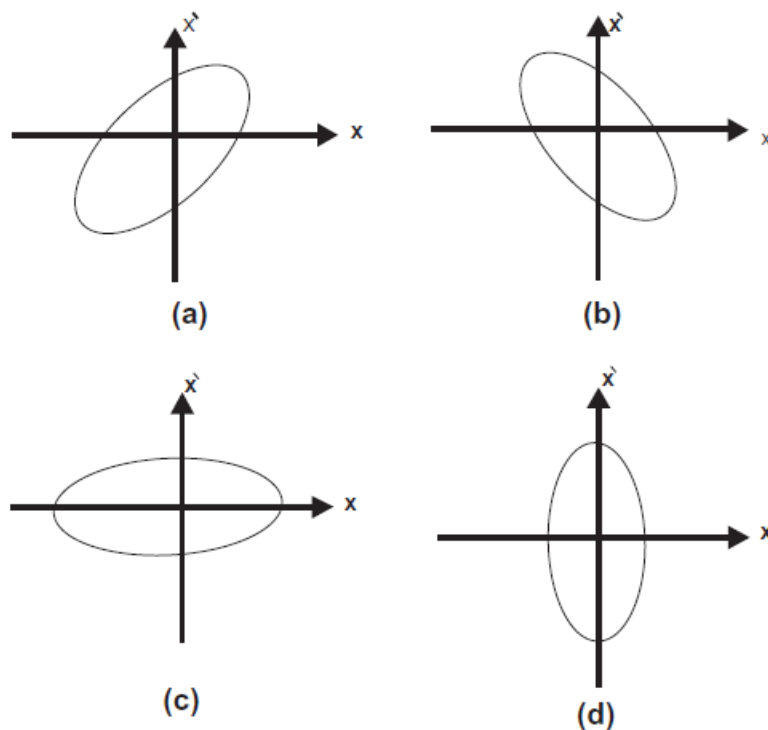
Figure 2. Different cases of two dimensional emittance patterns, with the corresponding beams as (a) divergent, (b) convergent, (c) parallel and (d) focused.
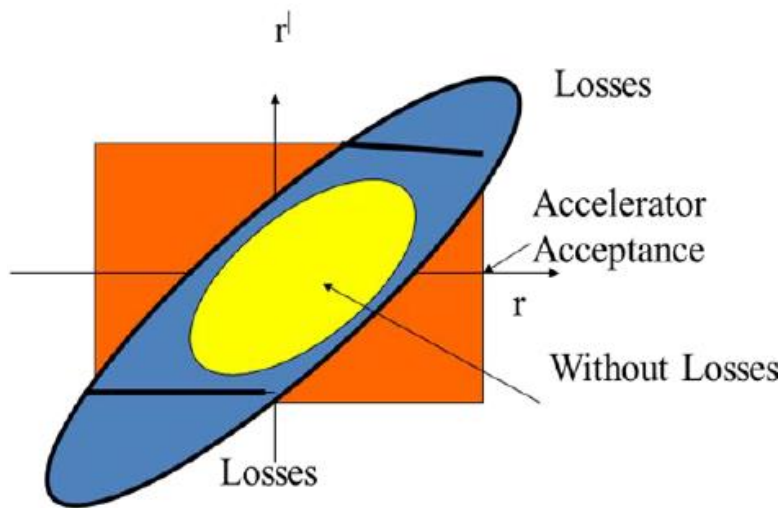

Figure 3. Accelerator acceptance with relation to the definition of emittance in phase space.

represents a schematic diagram that describes the acceptance of the accelerating system in phase space representation. To characterize the emittance of a beam in SIMION, it is necessary to create a user program, since the capability was not built into the original SIMION program. Each particle's coordinates and velocity components were tracked and logged. After the particles exited the simulation domain at the right of the mesh, their components were logged in a database, and the averages taken to find the emittance.
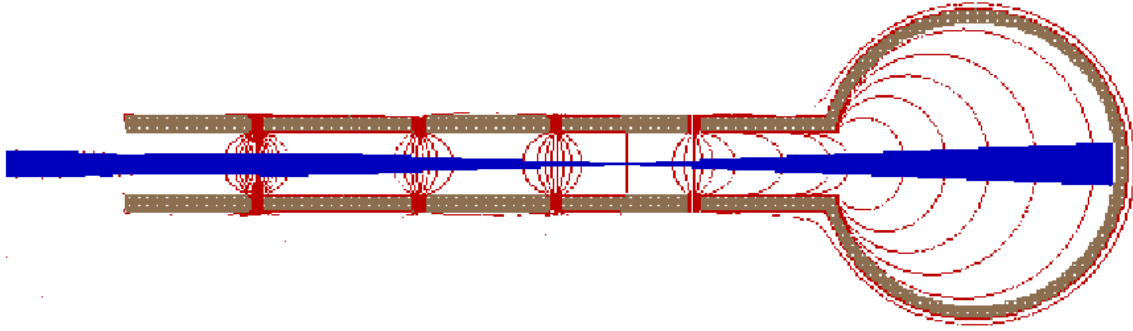
Figure 4. The Deceleration system with contours for singly charged argon ion trajectories.

In the present study, beam emittance was calculated by using the separate standard deviations of the positions (σ_y) and the elevation angles (σ_α) for singly charged argon ion trajectories;

$$\varepsilon = \sigma_y \cdot \sigma_\alpha \tag{3}$$

Standard deviation can be defined as

$$\sigma = \sqrt{\frac{1}{n-1}\sum_{i=1}^{n}\left(y_i - \overline{y}\right)^2} \tag{4}$$

where n is the number of repeated measurements, y_i is the individual values and $\overline{y}$ is the mean value of the repeated-values. For a fixed geometry of the deceleration lens system, the following calculations have been done with space charge of 10 mA.

SIMULATION PROCESS

The deceleration lens system was simulated using the ion optics simulation program SIMION (Dahl, 2000; Dahl et al., 1990). The program has been proven extremely useful in numerous applications. SIMION is an electrostatic lens analysis and design program that is capable of modeling charged particle optics problems with electrostatic and/or magnetic potential arrays. This program is used to simulate electrostatic and static magnetic devices for accelerating, transporting and otherwise manipulating beams of charged particles. For the purposes of this article, electrostatic fields only were modeled. In SIMION, five-point relaxation, a finite difference technique, is used as the iterative process to converge on the electric potential field solution for voltage contours and charged particle trajectories to be computed and plotted.

The lens system consists of a set of five cylindrical electrodes followed by a circle shaped electrode, all arranged along a common axis (Figure 4). As the beam traverses successive gaps between the electrodes, it encounters an increasing potential. The axial part of the electrostatic force is directed opposite to the direction of the incoming beam and has the net effect of reducing the energy of the beam.

Figure 5 shows the beam emittance and beam diameter as a function of the gap width for a decel voltage of 45 kv of a deceleration lens system for singly charged argon ion trajectories. It is clear from the figure that, a minimum gap width of 5 mm was obtained for its relation to beam emittance while an increase of the gap width was accompanied by an increase in beam diameter. Beam emittance and beam diameter as a function of the tube diameter for a decel voltage of 45 kv of a deceleration lens system for a singly charged argon ion trajectories was investigated (Figure 6). This figure shows that, there is a minimum of 26 mm of tube diameter for the relation between the inner tube diameter and beam emittance. Also, a minimum of 24 mm of inner tube diameter was obtained for the relation between the inner tube diameter and the beam diameter. Beam emittance and beam diameter for singly charged argon ion trajectories as a function of the focusing points for a decel voltage of 45 kv of a deceleration lens system were studied (Figure 7). A minimum of 455 mm was obtained at the outer exit of the deceleration lens system for the relation between the beam emittance and focusing points. While for the relation between the focusing points and beam diameter, a minimum of 460 mm was deduced. Figure 8 shows the influence of the deceleration voltage on both the beam emittance and beam diameter of a deceleration lens system for singly charged argon ion trajectories. It is found from this figure that, a minimum deceleration voltage of V_{decel} = 43 kV, was obtained for the relation between the deceleration voltage and beam emittance. Also, a minimum of V_{decel} = 49 kV is found for the relation between the deceleration voltage and beam diameter.
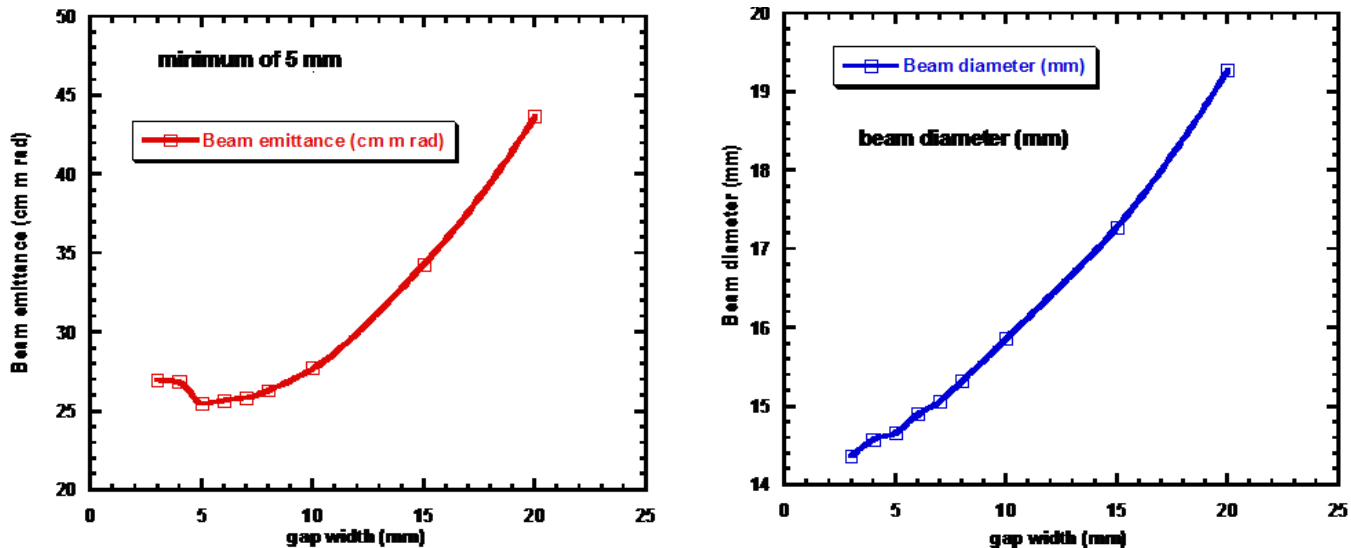
Figure 5. Beam emittance and beam diameter as a function of the gap width for a decel voltage of 45 kv of a deceleration lens system for a singly charged argon ion trajectories.
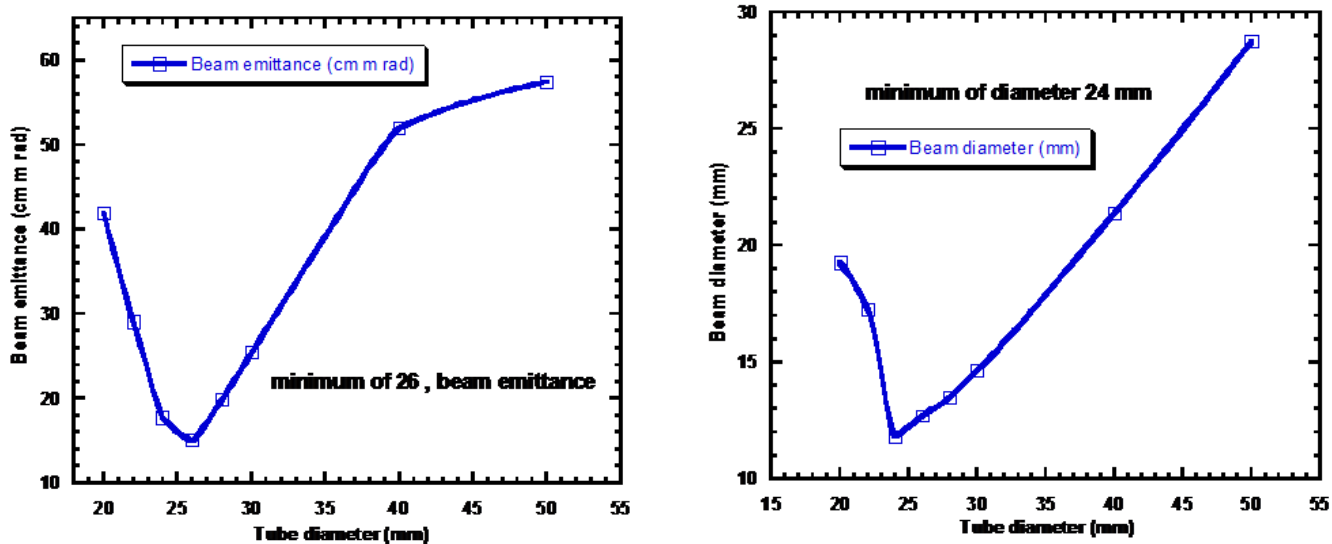

Figure 6. Beam emittance and beam diameter as a function of the tube diameter for a decel voltage of 45 kv of a deceleration lens system for singly charged argon ion trajectories.

Figure 9 illustrates a study of the influence of deceleration voltage on both beam emittance and beam diameter of a deceleration lens system for singly charged argon ion trajectories at the center of the experimental chamber. It was deduced from this figure that, a minimum deceleration voltage, V_{decel} = 47.5 kV occurred for the relation between the deceleration voltage and beam emittance at the center of the experimental chamber. In case of the relation between the deceleration voltage and beam diameter, increasing deceleration voltage applied to the deceleration electrode was accompanied by decreasing beam diameter.

CONCLUSIONS

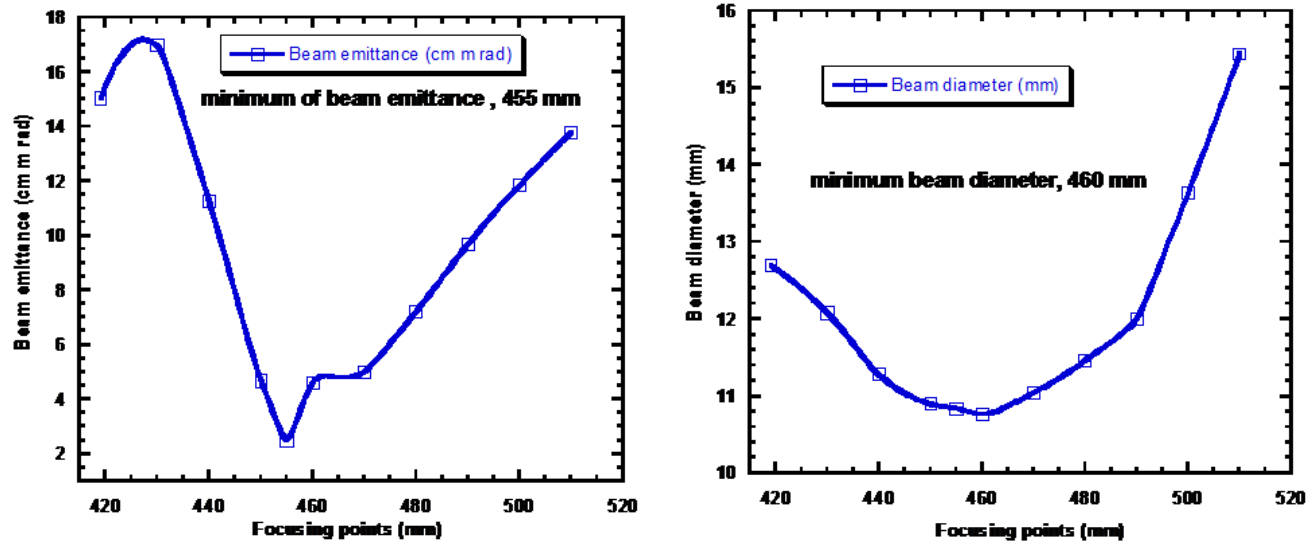These studies clearly demonstrate the necessity of providing means for varying the extraction gap to assure

Figure 7. Beam emittance and beam diameter as a function of the focusing points for a decel voltage of 45 kv of a deceleration lens system for singly charged argon ion trajectories.
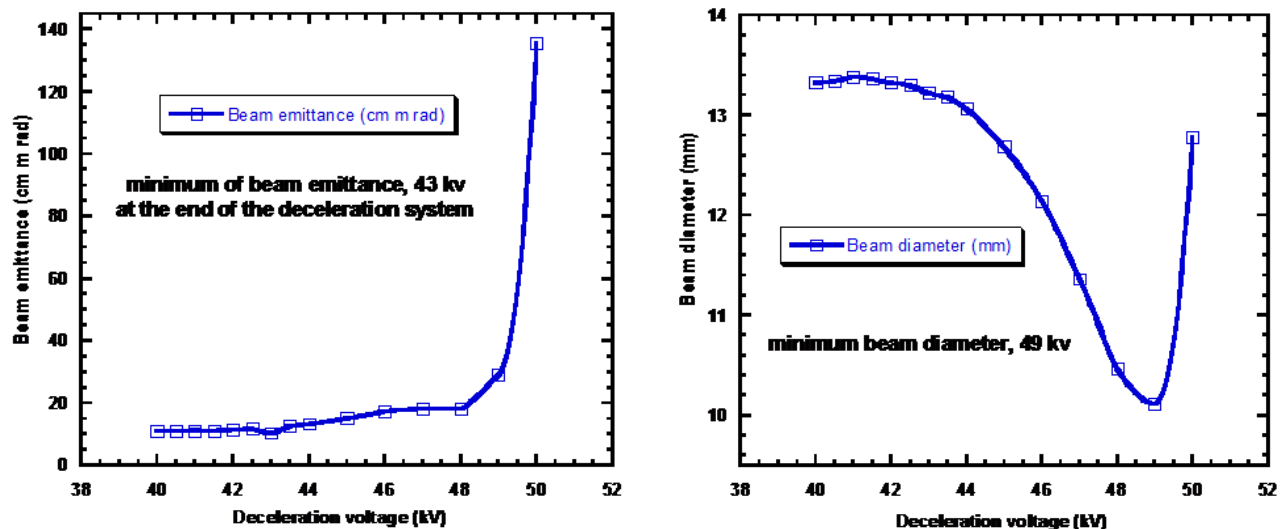

Figure 8. Influence of the deceleration voltage on both the beam emittance and the beam diameter of a deceleration lens system for singly charged argon ion trajectories.

high quality space-charge-dominated beams and also find the optimum parameters for the deceleration lens system which will be used experimentally in the next stage in isotope separation of ion beams of heavy ions. It was found that a minimum of gap width of 5 mm was obtained for the relation between the gap width and beam emittance while an increase of the gap width was accompanied by an increase of the beam diameter. Also, a minimum of 26 mm of tube diameter was obtained for the relation between the inner tube diameter and beam

emittance. Furthermore, a minimum of 24 mm of inner tube diameter was obtained for the relation between the inner tube diameter and the beam diameter. In further consequence, a minimum of 455 mm was obtained at the outer exit of the deceleration lens system for the relation between the beam emittance and focusing points. While for the relation between the focusing points and beam diameter, a minimum of 460 mm was deduced. It was found that a minimum of deceleration voltage V_{decel} = 43 kV, was obtained for the relation between the
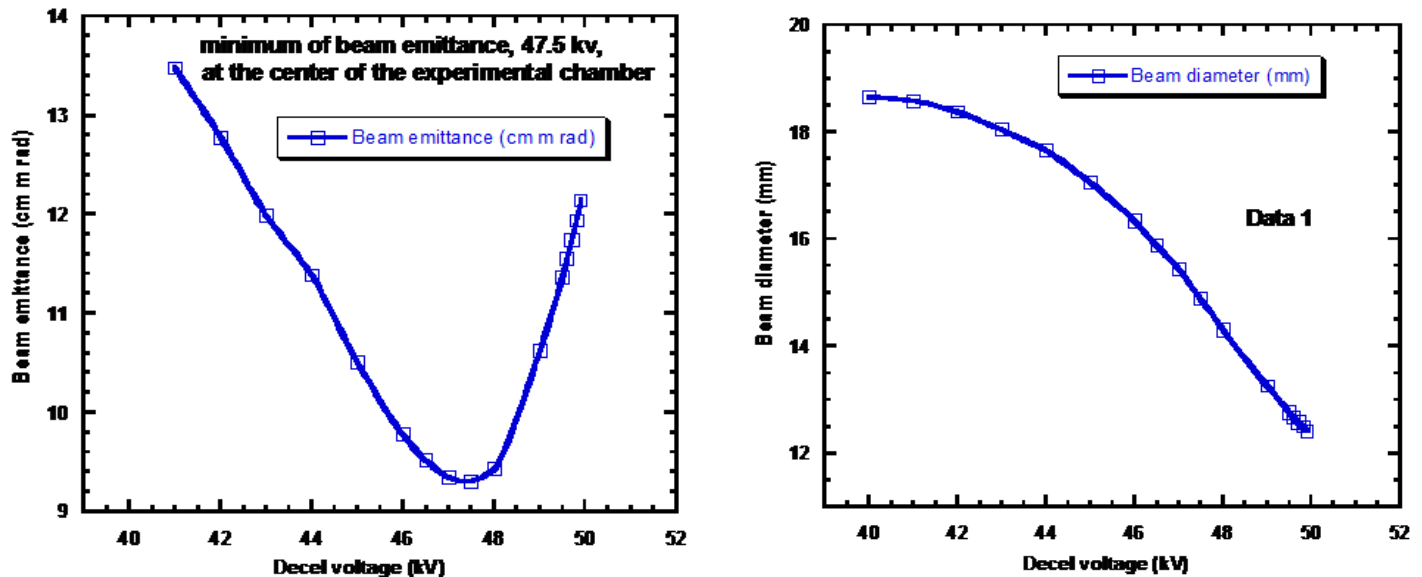
Figure 9. Influence of deceleration voltage on both the beam emittance and beam diameter of a deceleration lens system for singly charged argon ion trajectories at the center of the experimental chamber.

deceleration voltage and beam emittance. Also, a minimum, $V_{decel} = 49$ kV was found for the relation between the deceleration voltage and beam diameter. Finally, a minimum of deceleration voltage, $V_{decel} = 47.5$ kV was obtained for the relation between the deceleration voltage and beam emittance. In case of the relation between the decelration voltage and beam diameter, an increase of the deceleration voltage applied to the deceleration electrode was accompanied by a decrease of the beam diameter. From these results, it was concluded that the ion beam extracted from this ion source was decelerated to a certain amount of energy with a newly designed and siumlated deceleration system for injection of an isotope separator system.

Conflict of Interests

The author(s) have not declared any conflict of interests

REFERENCES

Abdelrahman MM, El-Khabeary H (2009). Study of three different types of plasma ion sources. Plasma Sci. Technol. 11(5). http://dx.doi.org/10.1088/1009-0630/11/5/17

Abdelrahman MM, Abdelsalam FW (2011). Computer investigation of ion beam optics for a Freeman type ion source system. Nucl. instruments methods in phys. Res. B. 269:1761–1766. http://dx.doi.org/10.1016/j.nimb.2011.04.110

Abdelrahman MM, Zakhary SG (2009). Simulation studies for ion beam extraction systems. Brazilian J. Phy. 39:2. http://dx.doi.org/10.1590/S0103-97332009000300005

Aitken D (2004). In: I.G. Brown (Ed.). The physics and technology of ion sources, John Wiley, New York.

Becker R, Herrmannsfeldt WB (1992). IGUN-A program for the simulation of ion extraction, including magnetic fields. Rev. Sci. Instrum. 63:2756. http://dx.doi.org/10.1063/1.1142795, http://dx.doi.org/10.1063/1.1142795

Boers JE (1993). A digital computer code for the simulation of electron and ion beams on a PC, IEEE Cat. No. 93CH3334-0 213. (PBGUNS is electron/ion optics simulation code, developed by Thunderbird Simulations, Garland, TX, USA).

Dahl DA (2000). SIMION 3 D Version 7.0 User's Manual INEEL-95/0403, Idaho National Engineering and Environmental Laboratory, I D 83415.

Dahl DA, Delmoreand JE, Appelhans AD (1990). SIMION PC/PS2 electrostatic lens design program. Rev. Sci. Instrum. 61:607. http://dx.doi.org/10.1103/PhysRevB.41.5763, http://dx.doi.org/10.1103/PhysRevB.41.5763

El-saftawy AM (2013). PhD. Thesis, Department of Physics Faculty of Science Zagazig University, Zagazig, Egypt.

Forrester AT (1988). "Large Ion Beams, Fundamental of Generation and Propagation "Wiley, New York. Humphries S Jr. (1990)."Charged Particle Beams", Wiley, New York.

Goncharov A (2013). The electrostatic plasma lens. Review of Scientific Instruments. 84:021101. http://dx.doi.org/10.1063/1.4789314, PMid:23464181, http://dx.doi.org/10.1063/1.4789314

Lee SY (1999). "Accelerator Physics", World Scientific, New York, USA.

Masood K, Iqbal M, Zakaullah M (2008). Emission characteristics of the thermionic electron beam sources developed at EBSDL. Nucl. Instrum. Meth Phys. Res. A 584:9. http://dx.doi.org/10.1016/j.nima.2007.09.049

Nikiforov S, Golubev V, Voronim G, Svinim M (1996). EPAC 96, Proceedings of the Fifth European Particle Accelerator Conference, Saint Petersburg.

Sise O, Ulu M, Dogan M (2005). Multi-element cylindrical electrostatic lens systems for focusing and controlling charged particles, Nucl. Instrum. Methods Phys. Res. A . 554 :114-131.

Sise O, Ulu M, Dogan M (2007). Characterization and modeling of multi-element electrostatic lens systems. Radiation Phys. Chem. 76:593–598. http://dx.doi.org/10.1016/j.radphyschem.2005.11.037

Spadtke P (1983). AXCEL-GSI, Interaktives Simulations programm zur Berechnung von Ionbahnen in electrostatischen Feldern unter Berncksichtigung der Raumladung, GSI Report 9.

Whealton JH, Bell MA, Raridon RJ, Rothe KE, Ryan PM (1988). Computer Modeling of Negative Ion Beam Formation. J. App Phys. http://dx.doi.org/10.1063/1.342078

Whealton JH, Whitson JC (1980). space-charge ion optics including extraction from a plasma, particle accelerators. 10:235-251.

Wielunski LS, Paterson GD, Bell JM, Clegg RE (2004). Production of Si+ and Cl+ ion beams from a Freeman type ion source using low toxicity and non-corrosive vapours as source gas Nucl. Instrum. Methods Phys. Res. B. 215:262–267.

International Journal of Physical Sciences

Related Journals Published by Academic Journals

- African Journal of Pure and Applied Chemistry
- Journal of Internet and Information Systems
- Journal of Geology and Mining Research
- Journal of Oceanography and Marine Science
- Journal of Environmental Chemistry and Ecotoxicology
- Journal of Petroleum Technology and Alternative Fuels